UNIVERSITY OF CALIFORNIA
RIVERSIDE

Quantitative FRET (qFRET) Technology for Determination of Protein Interaction Dissociation Constant in the Presence of Other Proteins and Development of Microfluidic Device

A Thesis submitted in partial satisfaction
of the requirements for the degree of

Master of Science

in

Bioengineering

by

Raphael Chih-Chung Kung

June 2015

Thesis Committee:
Dr. Jiayu Liao, Co-Chairperson
Dr. William H. Grover, Co-Chairperson
Dr. Jin Nam

The Thesis of Raphael Chih-Chung Kung is approved:

_____

_____

Committee Co-Chairperson

_____

Committee Co-Chairperson

University of California, Riverside

Acknowledgement

I would like to first thank my advisor, Dr. Jiayu Liao, for guiding me through a large portion of my higher academic life. His ongoing patience with experimental progress, and wealth of knowledge proved invaluable towards completion of every step. Dr. William H. Grover also has my heartfelt thanks for supervising the development of the microfluidics chip. Dr. Jin Nam, my final defense committee member, also deserves thanks for agreeing to assist me with my defense.

Next I thank my mentors and colleagues from my time in lab: Dr. Harbani Kaur Malik-Chaudry, Amanda Saavedra, Sophie (He) Qu, Jose Alanis, Michael (Zhehao) Xiong, and George Way for expert advice and technical support regarding experimental protocol; Nicole Duong, Jane Louie, Stephanie Kim, Annie Lee, and all the undergraduates who came into our lab for their assistance in helping carry out various stages of experimentation. Their support in nurturing my growth as a researcher cannot be quantified in value.

Lastly, I must give thanks to my family for supporting me throughout my foray into higher education, both financially and mentally. Special thanks goes towards my grandparents, half of whom have moved on since I decided to attend graduate school. They never quite understood what I was doing, but still believed in me with all their heart.

ABSTRACT OF THE THESIS

Quantitative FRET (qFRET) Technology for Determination of Protein Interaction Dissociation Constant in the Presence of Other Proteins and Development of Microfluidic Device

by

Raphael Chih-Chung Kung

Master of Science, Graduate Program in Bioengineering
University of California, Riverside, June 2015
Dr. Jiayu Liao, Co-Chairperson
Dr. William H. Grover, Co-Chairperson

Post-translational modification is one of the most vital functions at the cellular level in the human body. Ubiquitin and the Ubiquitin-like modifiers (Ubl's) are one class of post-translational modifier. They are involved in a variety of processes including transcription, DNA repair, and tumor progression. Each Ubl alters its target substrates through a 3 step enzymatic cascade of activation by E1, conjugation by E2, and ligation by E3. Our lab has developed a powerful Quantitative FRET analysis method to study the interactions at each step of the post-translational pathway. There are, however, less optimal components of the experimental procedure. The goal of my research is to increase the efficiency of lab protocol by determination of the effect of applying quantitative FRET measurements to unpurified proteins, and explore the possibility of integrating our quantitative FRET technology with microfluidics to enhance the efficiency of lab work.

Table of Contents

Chapter 1: Introduction **1**

1.1 Post translational modifiers 1

1.2 Ubiquitin 1

1.3 Small Ubiquitin-like Modifier 2

1.4 Förster Resonance Energy Trasfer 5

1.5 Microfluidics 13

Chapter 2: Quantitative FRET-based Determination of K_d Difference between Purified and Unpurified Protein Samples **16**

2.1 Introduction 16

2.2 Materials and Methods 18

2.3 Results 21

2.4 Discussion 24

Chapter 3: Development of a Microfluidics Chip for Automated Processing of Samples as a First Step towards Integrating Quantitative FRET into a Microfluidics Imaging Device **26**

3.1 Introduction 26

3.2 Materials and Methods 27

3.3 Results 42

3.4 Discussion 43

Chapter 4: Future Goals **44**

4.1 Regarding Protein Assay Studies 44

4.2 Regarding the Microfluidics Device 44

References **47**

List of Figures

Figure 1. **p.4**

SUMOylation pathway. SUMOylation is a 3 step enzymatic cascade involving an activating enzyme (E1), conjugating enzyme (E2), and ligating enzyme (E3). SUMO is first expressed in precursor form, where SENP, SUMO specific protease, cleaves off the C-terminal tail, exposing the diglycine motif for binding to SUMOylation pathways components. SUMO is first activated by Aos1/Uba2, its E1 activating enzyme, then transferred to Ubc9, its E2 conjugating enzyme. There are multiple E3 ligating enzymes, the most studied being the PIAS family of proteins. E3 recruits both substrate and the Ubc9-SUMO complex. SUMO then transfers to the substrate and modifies it. SENP will cleave SUMO so it returns to the beginning of the cascade.

Figure 2. **p.10**

Illustration of FRET when applied to protein interactions. A donor/acceptor pair is attached to two proteins believed to interact. If they do not, then excitation of the donor does not induce acceptor emission through FRET. If the proteins do interact, then excitation of the donor will induce acceptor emission from FRET.

Figure 3. **p.13**

Quantitative FRET method. A). Whole spectrum of CyPet-YPet emission. B). Direct emission of YPet at 530nm with 475nm excitation. C). CyPet emission spectra for determination of ratio α. D). YPet emission spectra for determination of ratio β. E). Equations used to determine K_d. $Em_{FRETmax}$ = signal when maximum amount of YPet is bound to CyPet, X = total YPet concentration, A = total CyPet concentration.

Figure 4. **p. 21**

Protein gels for CyPet-RanGAP1c and YPet-Ubc9. A). Lane 1, purified CyPet-RanGAP1c. Lane 2, purified YPet-Ubc9. B). Lanes 1-3, 0.2, 0.5, and 1.0µM unpurified CyPet-RanGAP1c. Lanes 4-6, 0.2, 0.5, and 1.0µM unpurified YPet-Ubc9.

Figure 5. **p.21**

Standard Curve of CyPet-RanGAP1c and YPet-Ubc9 emissions versus concentration.

Figure 6. **p.22**

Graph of Em_{FRET} for Purified CyPet-RanGAP1C plus YPet-Ubc9. CyPet-RanGAP1c concentrations fixed at 0.1, 0.2, 0.5, 1.0, and 1.5 µM. YPet-Ubc9 concentrations titrated from 0-3µM to reach signal plateau.

Figure 7. **p. 22**

Graph of Em_{FRET} for Purified CyPet-RanGAP1C plus YPet-Ubc9. CyPet-RanGAP1c concentrations fixed at 0.05, 0.1, 0.5, and 1.0 µM. YPet-Ubc9 concentrations titrated from 0-4µM to reach signal plateau.

Figure 8. **p. 24**

Bar graph comparing K_d between all concentrations of purified and unpurified protein samples. K_d is uniform between all concentrations, regardless of condition.

Figure 9. **p. 29**

Preliminary design of intersecting loops. Designed to have capacity to dilute two separate solutions, then mix them together.

Figure 10. **p.30**

Final design. A). Fluidic layer, designed for processing of 2 separate samples. B). Pneumatic layer, designed for actuation of valves to mix samples using 14 lines of control. C). Overlay of fluidic on pneumatic layer.

Figure 11. **p. 31**

Diagram of monolithic membrane valve operation. Fluid moves around in the top layer, but is stopped by discontinuities. Upon application of pressure from the pneumatic layer, the PDMS is drawn down, and fluid can continue to flow.

Figure 12. **p. 32**

Schematic of pin distribution. Out of 32 possible output pins, only 14 were used to control the microfluidic chip. Possible to expand to a 4 sample chip, run two separate 2 samples chips, or introduce higher complexity of commands in later design iterations while keeping same controller.

Figure 13. **p. 33**

Inverted photomask with chip design. Size of chip allowed for multiple copies on same pre-coated glass wafer containing glass, protective coating, and photosensitive coating.

Figure 14. **p. 34**

Photolithography. Standard method of imprinting design into glass substrate using UV light to develop a photosensitive layer for later etching.

Figure 15. **p. 35**

Etching process. A). Wafer with photoresist after applying chrome etch to remove protective chrome layer. B). Etching of wafer in hydrofluoric acid at 10μM/min. C). Etched wafer after removing photoresist and chrome layers.

Figure 16. **p. 36**

Final stages of fabrication. A). Drilling with the CNC mill. B). Fusing of the three layers: fluidic, PDMS, and pneumatic.

Figure 17. **p. 37**

Initial design of chip holder. Chip designed to sit on top of holder, which accounted for low flexibility of the tubing to fix tubes in place to ensure efficient transmission of pressure.

Figure 18. **p. 38**

Fully linked microfluidic set. From left to right: chip, holder, pressure tubing, solenoid array, Darlington arrays, rainbow wire, controller.

Figure 19. **p. 40**

Programs for Chip Control. A). Listener aligns computer lines of control to pins in the controller. B). Manual gives visual representation of which lines of control are active, and can manually activate them. C). OCW runes the scripts. D). Control has drop down menus for each chip loop, with relevant commands, and user input of how many iterations to run.

Figure 20. **p. 42**

Redesigned chip blueprint. Remodeled design attempts to integrate both pneumatic and fluidic layes onto the same side, allow of imaging of samples along the channels with little to no obstruction by tubing.

Figure 21. **p. 43**

Colored dye test for chip. Left loops loaded with yellow dye, right loops loaded with blue dye. Mixing both loops produced green dye.

Figure 22. **p. 46**

The inside of a Flexstation II 384. Important parts to replicate are: clear bottom well plate, excitation source, light detection module, and mirror orientation.

Chapter 1 Introduction

1.1 Post-Translational Modification

Within the human body, one of the most robust systems is that of cellular responses to stimuli. Transcription of DNA to RNA, followed by translation of RNA into proteins is one of those responses. Depending on the protein in question, further processing might be required for it to reach full functionalality. These are called post-translational modifications (PTM), covalent interactions that include phosphorylation, acetylation, methylation, glycosylation, and ubiquitination.[1] PTM's serve to prepare proteins for a specific function, modify their ability to interact with other proteins, control how they respond to changes in environment, and alter which state of activity the protein is in.

1.2 Ubiquitin

The first protein post translational modifier to have its functionality elucidated was ubiquitin, thanks to the efforts of Hershko, Ciechanover, and Rose.[2] Ubiquitin is a 74 amino acid, 8.5kDa protein found in most eukaryotic cells that modifies other proteins post-translation by ribosomes. It was discovered in 1975 by Goldstein, and was the first of its kind to be fully studied.[3] Most targets of ubiquitination, usually polyubiquitinated on their K48 lysine residue, find themselves heading for proteasomal degredation or lysosomal proteolysis.[4] There are cases where ubiquitination does not signal for degradation, like endocytosis in yeast cells, or DNA repair in eukaryotic cells.[5,6] Other modifiers like ubiquitin, such as Small Ubiquitin-like Modifier (SUMO) and Neural precursor cell expressed Developmentally Downregulated 8 (NEDD8), were identified as

having similar function and pathway to substrate modification, with varied sequence identity to ubiquitin, and amongst each other.[7] They are classified as the Ubiquitin-like modifiers, or Ubl's for short. Ubiquitin and the Ubl's generally require the use of a conserved mechanism, a three enzymatic complex cascade to link modifier to substrate. Due to the impact of PTM's on certain targets, the final enzymes in the cascade must be very specific with substrate recruitment.

1.3 Small Ubiquitin-like Modifier

Small Ubiquitin-like Modifier (SUMO), was first identified by Meluh and Koshland in 1995 as an inhibitor of MIF2, a gene that translates into a centromere protein required for mitotic spindle integrity.[8] It was later classified as a Ubl after being found attached to RanGAP1.[9] Four SUMO's are known, SUMO1-4. SUMO1 is 101 amino acids (~12kDa) long[10], while SUMO2 and SUMO3 are 92 and 93 amino acids long, respectively. They share only 20% sequence identity, but nearly fold in exactly the same conformation as ubiquitin. SUMO1 shares only 50% identity to SUMO2/3, while SUMO2 and SUMO3 are a 95% match. There are many cellular functions related to SUMO, including transcription, DNA repair, and nuclear transport.[11]

SUMOylation is quite similar to ubiquitination, which involves preparation after synthesis, a three step enzymatic cascade, and cleavage from the target substrate. Before entering the pathway, SUMO is first synthesized in a premature form. PreSUMO is processed by SUMO-specific proteases (SENP's) through proteolytic cleavage of the C-terminal tail, to expose the diglycine motif, which is the binding site of SUMO within its pathway. Mature SUMO is then ready for the three step SUMOylation pathway for

conjugation to substrates. First, SUMO forms a thioester bond in an ATP-dependant reaction between its diglycine motif, and a cysteine residue on the SUMO-specific E1 activating enzyme complex, Aos1-Uba2. Transfer from E1 to E2 links the carboxyl group on activated SUMO to the catalytic cysteine on the conjugating enzyme complex E2, Ubc9. An E3 ligating enzyme complex will recruit both substrate and the SUMO-Ubc9 complex. SUMO will then transfer to a lysine residue on the proximal substrate.[12] Three E3's exist for SUMO, PIAS1, RanBP2, and Pc2, with PIAS as the most documented due to its role in the JAK-STAT pathway.[13,14,15] Post-modification, SUMO is cleaved off by SENP, and returns to the beginning of the pathway. (**Figure** 1)

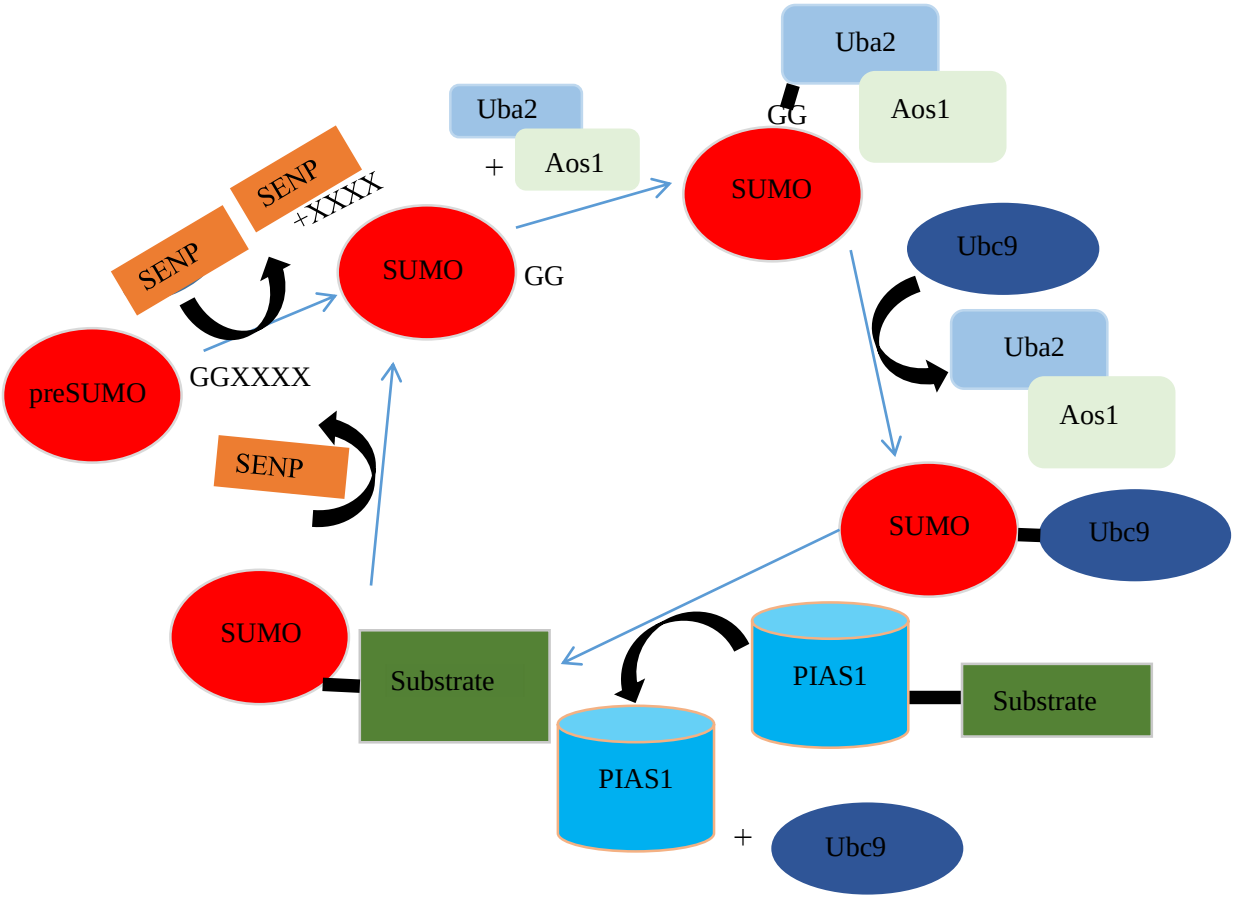

Figure 1. SUMOylation pathway. SUMOylation is a 3 step enzymatic cascade involving an activating enzyme (E1), conjugating enzyme (E2), and ligating enzyme (E3). SUMO is first expressed in precursor form, where SENP, SUMO specific protease, cleaves off the C-terminal tail, exposing the diglycine motif for binding to SUMOylation pathways components. SUMO is first activated by Aos1/Uba2, its E1 activating enzyme, then transferred to Ubc9, its E2 conjugating enzyme. There are multiple E3 ligating enzymes, the most studied being the PIAS family of proteins. E3 recruits both substrate and the Ubc9-SUMO complex. SUMO then transfers to the substrate and modifies it. SENP will cleave SUMO so it returns to the beginning of the cascade.

Due to the breadth of actions taken by SUMOylation targets, it is critical that mutations within the pathway do not occur. A mutation of SUMO4 done by Guo et al caused SUMO4 to negatively affect IκBα, the NFκB inhibitor, resulting in 5 times greater NFκB activity, which the authors suspect is highly suggestive of type 1 diabetes pathogenesis.[16] SUMO also participates in neurodegenerative diseases, like

Huntington's, Parkinson's, and Alzheimer's. The presence of SUMO3 activity in the brain helps to prevent the formation of amyloids in Alzheimer's, but once SUMOylation by SUMO3 starts decreasing, amyloid β peptide synthesis increases.[17] Quite a few cancers have mutated SUMOylation factors, including breast cancer.[18] One particular point to note is that the combined effects of SUMO and one of its E3 ligases, PIAS1, deal heavily in the regulation of p53, tumor suppressing gene, by repressing its transcriptional activity.[19] Since SUMO is so highly integrated into our body, it is imperative to study the SUMOylation pathway: all the mechanisms of its operation as known to the field, and potential additions that enhance or inhibit its activity.

1.4 Förster Resonance Energy Transfer

There are numerous pathways operating within the human body. From cell division to cell death, storage of digested glucose, to the transmission of electrical signals along nerve cells, each pathway is unique, and operates only under the right conditions. In order to produce medications or treatment methods, it is important to quantitatively understand the mechanisms of molecular interactions at the cellular level. A handful of techniques exist to study biochemical processes, including: Surface Plasmon Resonance (SPR), Isothermal Titration Calorimetry (ITC), Magnetic Resonance Imaging (MRI), Western blot, and Mass Spectroscopy. Techniques like MRI and mass spectroscopy are good for identifying ions and chemical groups, but lack the ability to monitor concentrations and detect protein interactions. Biochemical methodologies like western blot provide evidence of reaction through antibody staining, but cannot provide information regarding what occurs during an interaction. Lastly, there are the biophysical

techniques, which measure physical properties in order to elucidate reaction rates, concentration, and changes to proteins during interaction.

Isothermal Titration Calorimetry (ITC) is a technique for determination of changes in thermal energy due to reactions. One setup for ITC measurement is two thermally efficient solution chambers, one cell loaded with buffer for reference (control), and the other loaded with the target macromolecule in buffer for sample, surrounded by an adiabatic jacket. Sensitive circuits detect temperature change between the cells, and between each cell and the jacket upon injection of 5-10 µL of binding partner. A baseline amount of power is supplied to the reference cell, which changes to match the temperature of the reference cell to the sample cell after introduction of the binding partner (ligand). This change in heat is recorded. Ideally, the first few injections of ligand are completely bound to the target to establish a baseline of measurement. The remaining injections should show a sigmoidal response through the measured heat changes, until sample binding is fully saturated. K_a, the association constant, is determined through the equation:

$$Q = V_0 * \Delta H_b * [M]_t * K_a * [L] / (1 + K_a * [L])$$

where Q is the heat from adding ligand, V_0 is the cell volume, ΔH_b is the change in enthalpy, $[M]_t$ is the total concentration of the target macromolecule, and [L] is the concentration of free ligand. Precision is of utmost importance in ITC. Both ligand and macromolecule must be first dialyzed in buffer to remove any artifacts that might give off

false signals. They are further purified using filters and centrifugation to remove precipitate, then degassed to remove bubbles, which obstruct readings. A typical ITC experiment contains 15-20 ligand injections of 5-10μL added at intervals of 7-10 seconds. If the instrument used to inject ligand is bent through contact with the solution chamber, leakage of the ligand will occur, rendering measurements ineffective. After every injection, the solution is mixed at around 400 rpm. Collected data is corrected by removing the contributions of ligand being diluted in buffer, buffer being diluted in the macromolecule solution, and heat generated from stirring of the solutions after adding ligand. The final values are plotted as kcal/mol of ligand injected versus molar ratio of ligand to macromolecule.[20] There are several weaknesses to ITC as a result of the protocol. First, both binding partners need to be soluble in the buffer, else the technique cannot be used. In order to perform comprehensive experiments, a large amount of protein is also needed. Lastly, the high amount of precision needed throughout the experimental process means the measured results are easily ruined by tiny mistakes or deviations.

Surface Plasmon Resonance (SPR) is the biophysical technique tied to measurement of refractive index change on a metal sheet due to binding or dissociation incidents. The layout for SPR measurements is a glass prism sitting on a thin sheet of gold or other appropriate metal, with ligands fixed on the opposite side. A beam of light is shone through the prism onto the gold sheet, and the reflected light is captured using a detector. When a solution of known conjugators of the fixed ligand is run along the seeded surface, binding events induce change in the refractive index, shifting the angle of

reflectance and resonance angle. Surface plasmons are waves of oscillating surface charge density travelling along the surface of metals. The plasmon is resonantly excited by light at a well-defined angle of incidence, where the wave vector of light in the plane of the sensor surface matches that of the plasmon. This resonance results in energy loss for reflected light, seen as a sharp minimum in the angle-dependent reflectance, which is the measured signal. SPR can be used to determine K_D through the equation, $K_D = k_-/k_+$, where k_- is the complex dissociation rate, and k_+ is the complex association rate. These are determined through:

$$\frac{dR}{dt} = k_+ * f_0 * R_{sat} - (k_+ * f_0 + k_-) * R$$

where R is the biosensor response, $f_0 \equiv [L]$, the ligand concentration, and R_{sat} is the biosensor response at complete saturation of the binding sites.[21] SPR is not without its own difficulties though. The immobilized binding sites need to have high specificity, else binding may reduce activity of the protein, even bind in the wrong location or orientation. Additionally, SPR cannot differentiate between specific and non-specific binding, and non-specifically bound proteins are not guaranteed to be removed with the wash for eluting normal binding partners. The size limit of SPR is 20kDa, anything smaller is hard to detect unless a significant amount in densely bound to the surface. The surface is also the only area where detection occurs, which leaves most of the SPR chips unused for sensing.[22]

The last major biophysical method is fluorescent tagging, attaching fluorescent markers to targets of study for observance of intensity, determination of intermediates, or localization, which has helped make large advances in imaging cells and other biological structures.[23] Of the two kinds available, encoding fluorescent protein into target DNA is more effective than chemically induced tagging of fluorescent molecules, because of the lower risk to change the structure of the target. Furthermore, fluorescent protein tags are effective for studies on subcellular mechanisms, from metabolite tracking in biochemical pathways to protein-protein interactions in vitro and in vivo.[24,25]

Förster Resonance Energy Transfer (FRET) is a nonradiative energy transfer process by which energy from an excited state donor transfers to a ground state acceptor, given that the distance between them is 1-10 nm, and the emission spectrum of the donor overlaps with the excitation spectrum of the acceptor.[26, 27] The rate constant of energy transfer is:

$$k_T = r^{-6*}\kappa^{2*}J*n^{-4*}k_F \text{ x } 8.71 \text{ x } 10^{23} sec^{-1}$$

Where r is the distance between the centers of the donor and acceptor, κ^2 is the dipole-dipole orientation factor, J is the integral of spectral overlap between donor emission and acceptor excitation, n is the refractive index of the medium, and k_F is the rate constant of fluorescent emission of the donor. The efficiency, E, distance at which transfer efficiency is 50%, R_0, and associated variables are expressed as:

$$E = R_0^6 / (R_0^6 + r^6)$$

$$R_0 = (J*\kappa^2*Q_0*n^{-4})^{1/6} * 9.7 \text{ x } 10^3 \text{ Å}$$

$$J = \left(\int F(\lambda) * \epsilon(\lambda) * \lambda^4 * d\lambda\right) \Big/ \int F(\lambda) * d\lambda$$

Q_0 is the quantum yield of the donor fluorescence in the absence of the acceptor, F(λ) is the fluorescence intensity of the donor at wavelength λ, and ϵ(λ) is the extinction coefficient of the acceptor.[28]

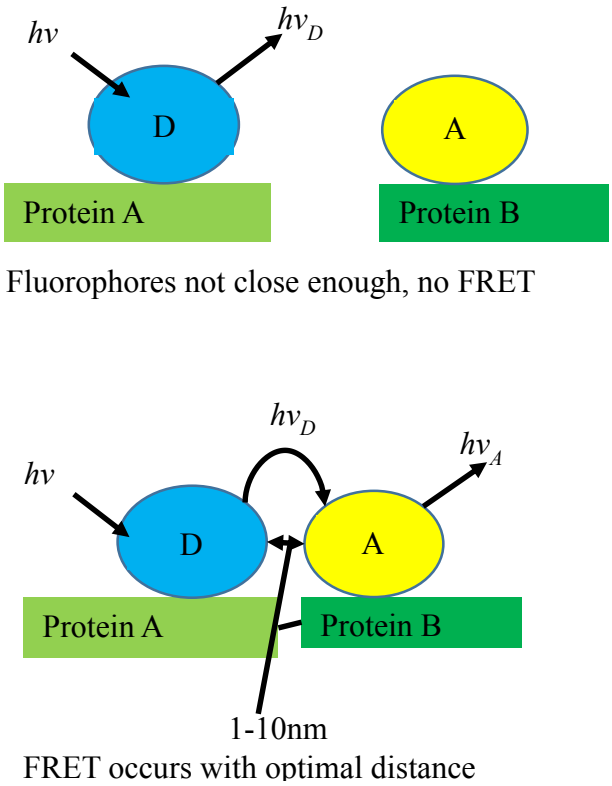

Figure 2. Illustration of FRET when applied to protein interactions. A donor/acceptor pair is attached to two proteins believed to interact. If they do not, then excitation of the donor does not induce acceptor emission through FRET. If the proteins do interact, then excitation of the donor will induce acceptor emission from FRET.

Due to the transfer efficiency of FRET being reliant upon the distance between donor and acceptor, FRET is a popular choice for studying protein-protein interactions. Quantitative FRET analysis for determination of reaction rate constants is achieved through a number of analytical methods involving determination of FRET efficiency, or

calculating change between FRET indexes, relative values of measured fluorescence signals that change with increasing and decreasing FRET. The efficiency equations vary by the amount of cross talk removed, and level of measured FRET signal correction, increasing in complexity with increase in correctness. Each FRET index is tailored to a specific end, thereby making comparison between results of individual indexes difficult. The current methodologies either become more convoluted to achieve higher accuracy of results, or rely upon abstract ratios to evaluate FRET quantitatively, making comparison of results a hassle.[34]

A method of quantitative FRET analysis for determination of the dissociation constant, K_d, from FRET emission spectra was developed by a previous grad student in our lab. Excitation of a mixture of CyPet-SUMO1 and YPet-Ubc9 at donor excitation 414nm produces an emission spectrum with peaks at 475nm and 530nm, corresponding to the donor and acceptor emission wavelengths. The total emission observed at 530nm (Em_{total}), the emission wavelength of the acceptor, is composed of three parts: direct donor emission (FL_{DD}), direct acceptor emission (FL_{AA}), and acceptor emission from FRET (Em_{FRET}). Direct donor emission, emission at 530nm from the donor being excited at 414nm, is proportional to the peak emission at 475nm from the same excitation, represented by constant α. Direct acceptor emission, emission at 530nm of the acceptor when excited at 414nm, is proportional to the emission at 530nm given 475nm excitation, represented by the constant β. α and β were determined to be 0.33 and 0.026 when calculated from pure CyPet-SUMO1 and YPet-Ubc9, respectively. After removing the direct emissions of donor and acceptor, the remaining signal is considered true FRET-

based acceptor emission, Em_{FRET}.[30] This quantitative FRET method has been employed to determine all of the reaction rate constants for the SUMOylation pathway, as well as high throughput screening of potential inhibitors.[35-40] All of the measurements thus far have been performed with fully purified proteins, yet the purification process is not perfect. Certain proteins, like the E3 sUMO ligating enzyme PIAS1, are difficult to purify a high concentration of. Other proteins are truncated or degraded as a result of the purification process. Additionally, some contaminant proteins are expressed with the histidine tag we use for column chromatography separation of our proteins from the rest of cell lysate. The first challenge of my work involves measuring the FRET emission from protein samples before undergoing column chromatography, to determine if the emission observed from extracted, unpurified protein is comparable to that of fully purified protein. If this proves effective, we can employ this methodology when encountering other difficult proteins across the human genome.

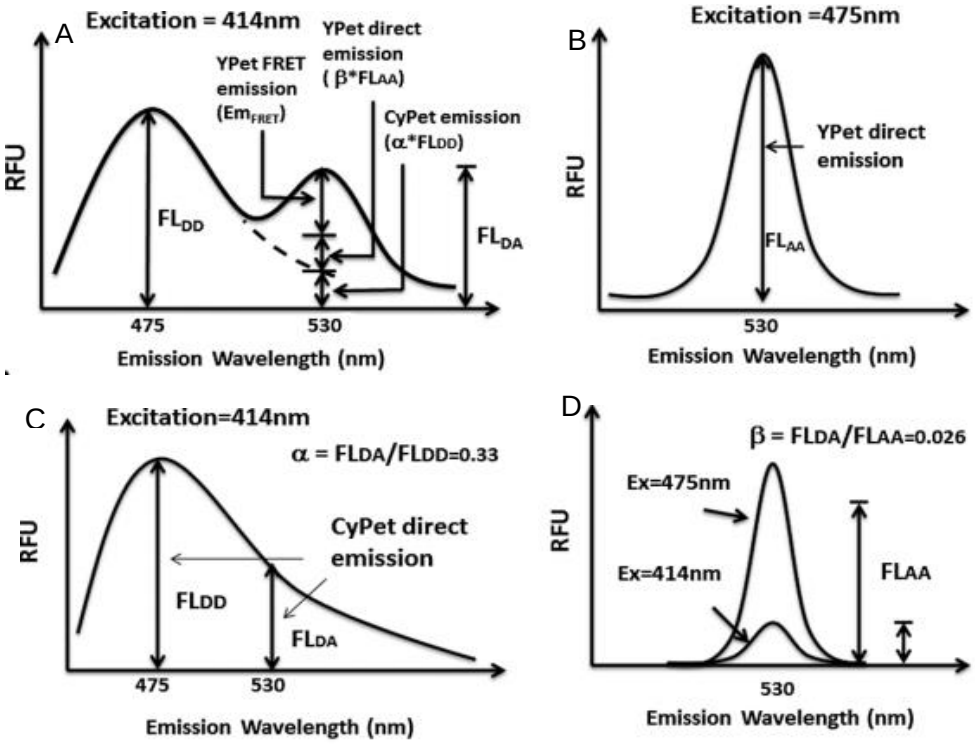

E $Em_{FRET} = Em_{total} - \alpha(Em_{475/414}) - \beta(Em_{530/}475)$

$$Em_{FRET} = Em_{FRETmax}\ (1 - \frac{2Kd}{X - A + Kd + \sqrt{(X - A - K_d)^2 + 4K_dX}})$$

Figure 3. Quantitative FRET method. A). Whole spectrum of CyPet-YPet emission. B). Direct emission of YPet at 530nm with 475nm excitation. C). CyPet emission spectra for determination of ratio α. D). YPet emission spectra for determination of ratio β. E). Equations used to determine K_d. $Em_{FRETmax}$ = signal when maximum amount of YPet is bound to CyPet, X = total YPet concentration, A = total CyPet concentration.

1.5 Microfluidics

Microfluidics is the field of science dealing with the observation and control of around microliter volumes of fluid through channels and valves of nano- to micrometer length and thickness. From early on, microfluidics centered on exploiting the nature of their size for the sake of expanding the horizons of science. Compactness of devices translated into less reaction volume, faster processing times, and higher throughput as a

result. The first chips were designed from glass and silicon, for the purpose of performing small-scale experiments like capillary electrophoresis.[41] These were derived from microelectronics and MEMS designs, which fell short when applied to biological studies. The physical and chemical properties of silicon especially proved to have poor optical properties, expensive fabrication, and rigidity that did not favor cell growth.[42]

Poly(dimethylsiloxane) (PDMS), an elastiomer, proved to be a more applicable material for microfluidic fabrication, capable of forming a tight seal with itself, and even the predecessor materials glass and silicon, when oxidized.[43] Soft lithography methods for fabrication of chip design arose from the advent of membranes designed from polymers like PDMS.[44] As opposed to creation of channels by depositing layers of materials slowly, or imprinting a design onto a photoresistant layer, and etching with hydrofluoric acid, soft lithography molds the chip material, PDMS, around a premade scaffold for considerably less hassle. In 2000, the Quake group introduced monolithic microfluidic chips made by soft lithography.[45] By switching the composition of all parts, valves and pumps included, to PDMS, the required area of fabrication was reduced even more, while retaining the properties of PDMS that made it suitable for biological applications. Expanding on the reduction of size, Thorson et al proved that a denser amount of valves could be factored into microfluidic chips, allowing for multitudes greater complexity to assays.[46] The next novel advancement in microfluidics arrived as monolithic membrane valves and pumps. Channel fabrication from soft lithography was optioned out for an unaltered piece of PDMS sandwiched between etched glass pieces. As opposed to their wholly PDMS counterparts, monolithic membrane valves are by

default closed, allowing for parallel operation of innumerable sets of valves.[47] Additionally, by placing the valves in series, a diaphragm valve can be created to transport a fixed amount of fluid through. These properties make the monolithic membrane valves and pumps ideal for the laboratory environment, where diluting known amounts of solution is a necessary procedure.

Microfluidics has a wide range of applications throughout the sciences. One branch has returned to the electrical origins of the circuitry mimicking microchip.[48] Another utilizes the scaling of microfluidic channels to make submicrometer resolution inkjet printing.[49] Even seeding of cells for controlled growth of tissues using a biodegradable microfluidic scaffold is a possibility.[50] Towards a more cellular and biological direction, one group was able to isolate circulating tumor cells in the blood of cancer patients using microposts.[51] And, although the route is not complete, soon high throughput screening will become a facet of the spectrum of applications for microfluidic technology.[52] Several examples detail the combination of fluorescence and microfluidics, but none of them utilize our quantitative FRET technology. Therein, I introduce the second portion of my project, to unify our lab's quantitative FRET technology with microfluidics, to expedite the processing speed of samples for FRET measurements, and increase the breadth of functions microfluidics can be applied to.

Chapter 2. Quantitative FRET-based Determination of K_d Difference between Purified and Unpurified Protein Samples

2.1 Introduction

The human body is full of biological processes that help it function on a day to day basis. Proteins are central to the operation of many biological processes, and there exist a number of techniques to study protein interactions, including SPR and western blot. It is however, easy to pick up contaminants during the process of expressing and collecting proteins for assays. Thus, the ability to perform experimental studies while ignoring the effect of contaminants and unexpected changes is invaluable. Fluorescence tagging is one such technique used for experimentation with minimal invasiveness to the activity of proteins. Using it, we can identify values like K_d, the dissociation constant, for assessment of the interactions between proteins of non-covalent nature. Other methodologies like SPR and ITC can be used to obtain K_d, but they are quite complex to execute, or are have limitations to the scope of measurement available.

Post-translational modification sits on the crossroads of a wide variety of cellular processes in the body. Without the efforts of ubiquitin and the ubiquitin-like modifiers, many proteins would be unable to perform their designated function, and the body would destabilize through disease. The Small Ubiquitin-like Modifier (SUMO) family has 4 members of approximately 100 amino acid length.[10] They process a variety of proteins, including those involved in transcription, nuclear transport, and DNA repair.[11] Like ubiquitin, SUMO conjugation to target substrates occurs through an enzymatic cascade of E1 (activating enzyme), E2 (conjugating enzyme), and E3 (protein ligase). SUMOylation

begins with the cleavage of preSUMO by SUMO specific protease (SENP), to expose the diglycine motif on the C-terminal for binding to cascade elements. Aos1-Uba2, the E1 heterodimer, adenylates SUMO in the presence of ATP and Mg^{2+}, leading into thioester bond formation between a cysteine residue in Uba2's active site and the exposed glycine residue of SUMO's C-terminal.[28] SUMO is then transferred to the active site cysteine residue of Ubc9, it's E2, conjugating enzyme. E3, the protein ligase, one of the more well-known being PIAS, is responsible for recruitment of Ubc9-SUMO and the substrate.[19]

Förster Resonance Energy Transfer (FRET), is one of the techniques used to calculate K_d. It is the phenomena by which energy is transferred from an excited state donor to a ground state acceptor, given that the emission spectrum of the donor intersects with the excitation spectrum of the acceptor, and they are within 1-10nm proximity. It has a variety of uses, including being a reliable sensor of molecular activity in vitro and in vivo.[31-33] The signal strength correlates to the amount of donor-acceptor pairs active, which makes it a good quantitative measure of how much interaction happens. Our lab's utilization of the engineered FRET pair CyPet and YPet on the SUMOylation pathway allowed for insights into developing a method to quantify the interactions within the pathway.[30, 35-40] All of the prior work our lab has done involved fully purified proteins, yet there have been a few difficulties with purification procedure affecting the proteins being expressed. Herein we report on the difference not purifying our proteins has on the efficiency of our quantitative FRET technology.

2.2 Materials and Methods:

Protein Expression

BL21 *Echerichia coli* cells were transformed using two pET28(b) vectors, one encoding CyPet-RanGAP1c, the other encoded with YPet-Ubc9. The transformed bacteria were plated onto 50µg/mL kanamycin LB agar plates, and grown for 16 hours. Single colonies were picked up and inoculated with 2xYT media containing 1mM kanamycin, and inoculated for 3 hours. Expression of our poly-histidine-tagged recombinant proteins was induced with 0.1mM isopropyl β-D-1-thiogalactopyranoside (IPTG), and left to continue overnight. Bacterial cells were collected by centrifugation at 8,000 rpm for 5 minutes at 4℃, resuspended in binding buffer (20mM Tris-HCl pH 7.4, 500mM NaCl, and 5mM imidazole), and sonicated with an ultrasonic liquid processor (Misonix). Cell lysates with recombinant proteins were centrifuged at 35,000xg for 30 minutes to remove cell fragments. A few milliliters of lysate were collected for testing later. The polyhistidine-tagged recombinant proteins were purified from bacterial lysate using Ni^{2+}-NTA agarose beads (QIAGEN) in columns, and washed by three distinct wash buffers: Wash buffer 1 (20mM Tris-HCl pH7.4, 200mM NaCl), Wash buffer 2 (20mM Tris-HCl pH 7.4, 1.5M NaCl, 5% Triton X-100), and Wash buffer 3 (20mM Tris-HCl pH 7.4, 500mM NaCl, 20mM imidazole). Our protein was eluted from the columns using elution buffer (20mM Tris-HCl pH 7.4, 200mM NaCl, 250mM imidiazole). The proteins were then allocated into dialysis tubing, and suspended in dialysis buffer (20mM Tris-HCl pH 7.4, 50mM NaCl, 1mM DTT). Purity of the proteins was confirmed by SDS-PAGE and Coomassie blue staining, concentration of the purified protein determined by

Coomassie Plus Protein Assay (Pierce) (**Figure 4)**, and unpurified concentrations determined by fitting to standard curve of concentration versus emitted fluorescence. (**Figure 5**)

FRET measurement

Purified recombinant CyPet-RanGAP1c and YPet-Ubc9 were incubated and mixed at 37˚C in Tris buffer (20mM Tris-HCl pH 7.5, 50mM NaCl, 1mM DTT) to 60µL final volume. CyPet-RanGAP1c concentration was fixed at 0.1, 0.2, 0.5, 1.0, and 1.5 µM, while YPet-Ubc9 concentrations were varied from 0-3µM. Unpurified CyPet-RanGAP1c and YPet-Ubc9 had their concentrations measured by Fluorescence standard curve derived by a previous grad student. CyPet-RanGAP1c concentration was fixed at 0.05, 0.1, 0.5, and 1.0 µM, and YPet-Ubc9 concentrations were varied from 0-4µM. The mixtures were examined by a multi-well plate reader, Flexstation II 384 (Molecular Devices)

After loading onto a 384 well plate, and insertion into the Flexstation II 384, mixtures were excited at 414nm and 475nm for measurement of emission spectra. Emission at 475nm from 414nm excitation (FL_{DD}), emission at 530nm from 414nm excitation (Em_{total}), and emission at 530nm from 475nm excitation (FL_{AA}) were collected. The emission observed at 530nm consists of three parts: direct CyPet-RanGAP1c emission, direct YPet-Ubc9 emission, and the YPet-Ubc9 emission from FRET (Em_{FRET}). To complete determination of Em_{FRET}, we calculated α and β using a separate set of samples. CyPet-RanGAP1c was loaded into wells at concentrations of 0.1, 0.2, 0.5, 1, and 1.5µM. Excitation at 414 nm gave us values for emission at 475nm and 530nm. By

dividing the 530nm emission by the 475nm emission, we get α, which helps us determine the contribution of direct CyPet emission to the observed 530nm peak. Next YPet-Ubc9 was loaded into wells at concentrations 0.2, 0.5, 1, 2, 3, and 4μM and excited at 414nm and 475nm for collection of the 530nm emission value. β was obtained by dividing the 530nm emission from 414nm excitation by the 530nm emission from 475nm. The value of Em_{FRET} for each mixture of CyPet-RanGAP1c and YPet-Ubc9 was determined by removing background signal from a blank plate measurement, the plugging α, β, FL_{DD}, and FL_{AA} from each one into the equation $Em_{FRET} = Em_{total} - FL_{DD}(\alpha) - FL_{AA}(\beta)$. The datasets for YPet-Ubc9 concentrations and corresponding Em_{FRET} values were fitted in Prism 5 (Graphpad Software) to find values for $Em_{FRETmax}$ and K_d. A method of nonlinear regression was selected to process the triplicate Em_{FRET} versus YPet-Ubc9 data using the custom equation developed in our lab:

$$Em_{FRET} = Em_{FRETmax}\left(1 - \frac{2Kd}{X - A + Kd + \sqrt{(X - A - K_d)^2 + 4K_dX}}\right)$$

In Prism, the initial values for parameters Em_{FRET}, K_d, and A are set to 1.0. X correlates to the YPet-Ubc9 concentration, and A correlates to the CyPet-RanGAP1c concentration. The results appear as a mean ± standard deviation.

2.3 Results

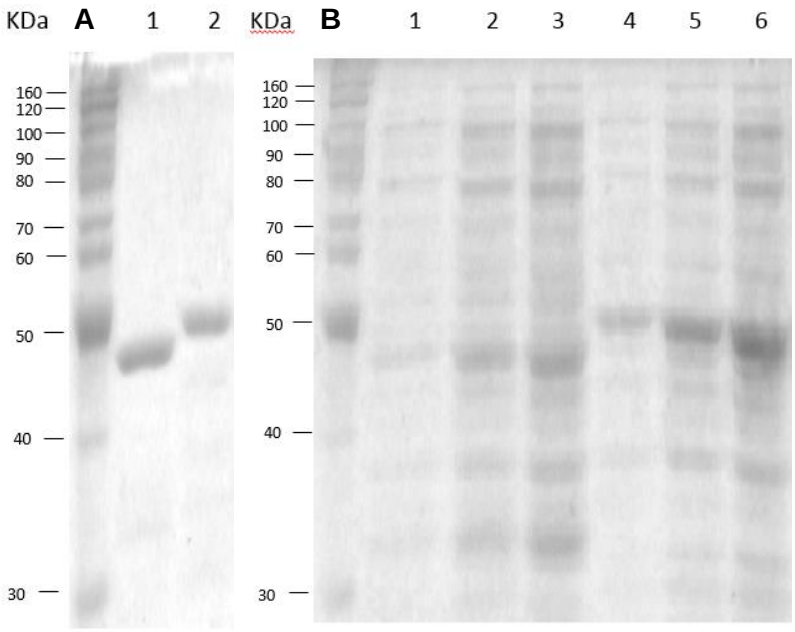

Figure 4. Protein gels for CyPet-RanGAP1c and YPet-Ubc9. A). Lane 1, purified CyPet-RanGAP1c. Lane 2, purified YPet-Ubc9. B). Lanes 1-3, 0.1, 0.5, and 1.0µM unpurified CyPet-RanGAP1c. Lanes 4-6, 0.1, 0.5, and 1.0µM unpurified YPet-Ubc9.

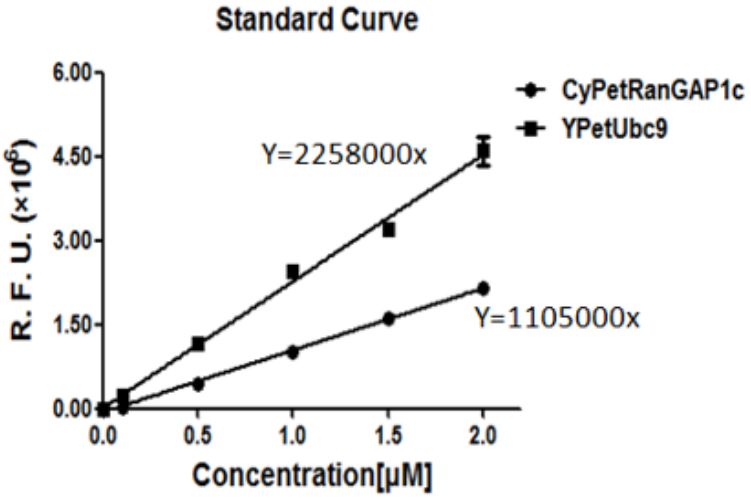

Figure 5. Standard Curve of CyPet-RanGAP1c and YPet-Ubc9 emissions versus concentration. Used to determine the concentrations of unpurified proteins.

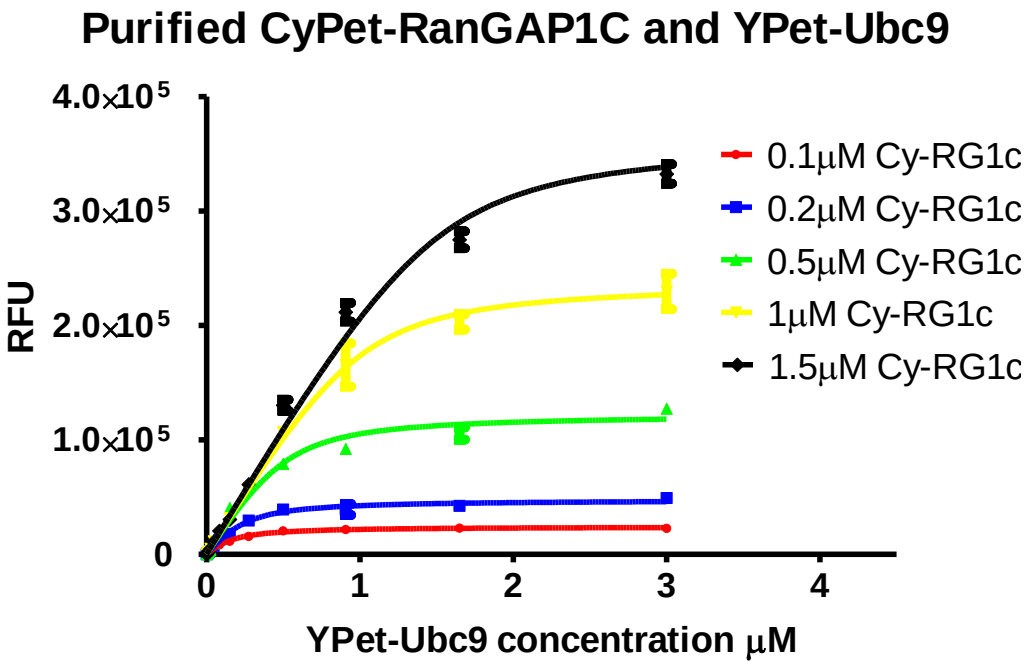

Figure 6. Graph of Em_{FRET} for Purified CyPet-RanGAP1C plus YPet-Ubc9. CyPet-RanGAP1c concentrations fixed at 0.1, 0.2, 0.5, 1.0, and 1.5 μM. YPet-Ubc9 concentrations titrated from 0-3μM to reach signal plateau.

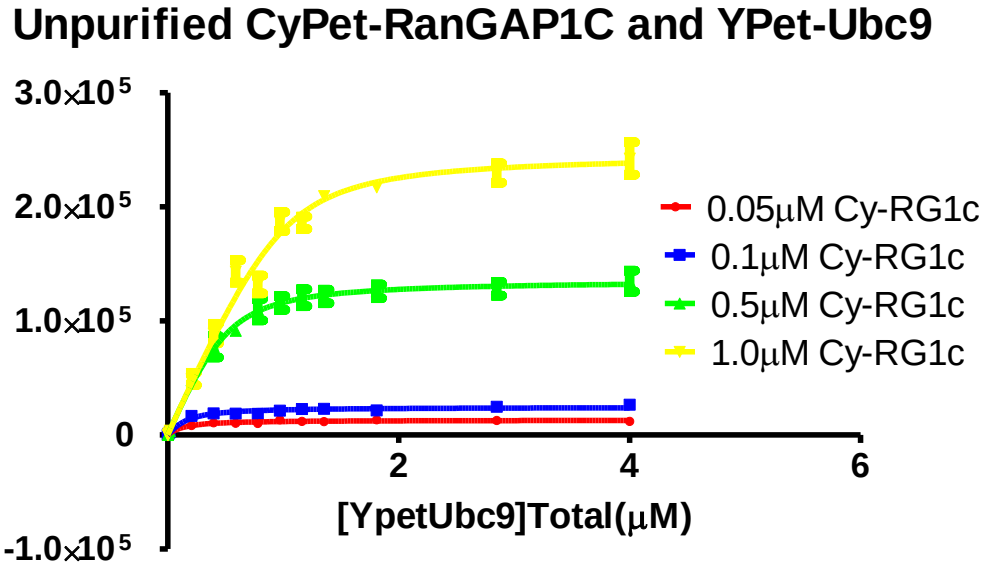

Figure 7. Graph of Em_{FRET} for Purified CyPet-RanGAP1C plus YPet-Ubc9. CyPet-RanGAP1c concentrations fixed at 0.05, 0.1, 0.5, and 1.0 μM. YPet-Ubc9 concentrations titrated from 0-4μM to reach signal plateau.

CyPet-RanGAP1c (µM)	K_d (µM)	$Em_{FRETmax}$ (x 10^5 RFU)
0.1	0.1010 ± 0.01534	2.428 ± 0.07133
0.2	0.0986 ± 0.01629	4.773 ± 0.1295
0.5	0.0936 ± 0.02764	12.26 ± 0.4486
1.0	0.1013 ± 0.03930	23.82 ± 0.9647
1.5	0.1103 ± 0.04745	36.19 ± 1.536

Table 1: Results for purified CyPet-RanGAP1c + YPetUbc9 FRET measurement

CyPet-RanGAP1c (µM)	K_d (µM)	$Em_{FRETmax}$ (x 10^5 RFU)
0.05	0.1016 ± 0.02443	1.308 ± 0.04085
0.1	0.09988 ± 0.02390	2.447 ± 0.07524
0.5	0.09616 ± 0.02348	13.57 ± 0.3915
1.0	0.1001 ± 0.02919	24.63 ± 0.7893

Table 2: Results for unpurified CyPet-RanGAP1c + YPetUbc9 FRET measurement

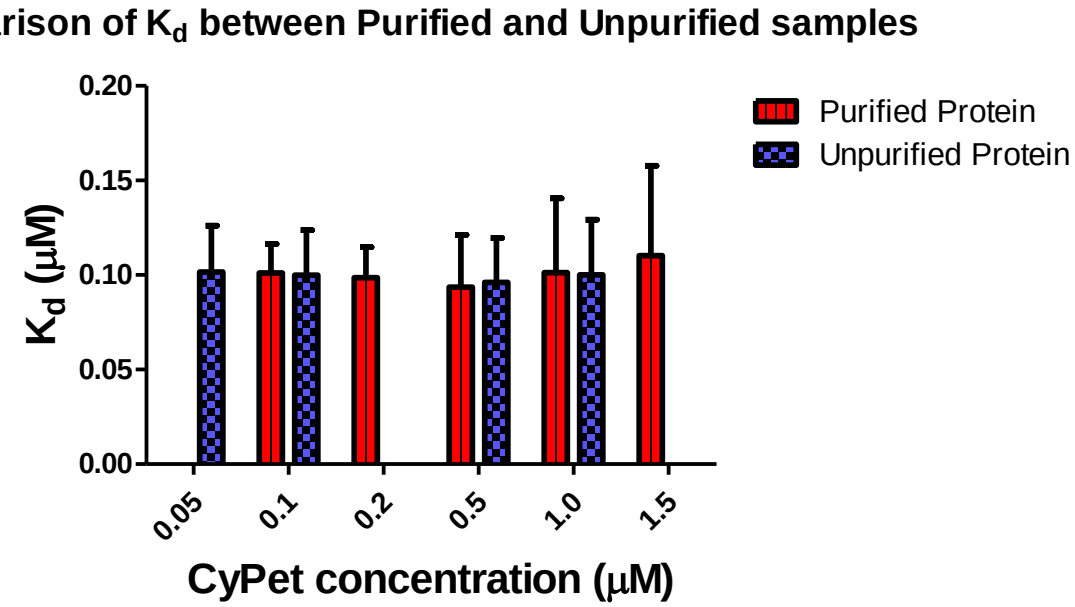

Figure 8. Bar graph comparing K_d between all concentrations of purified and unpurified protein samples. K_d is uniform between all concentrations, regardless of condition.

2.4 Discussion

Here we report having determined the effect of not fully purifying protein samples on our lab's quantitative FRET method for determination of the dissociation constant, K_d. The highly efficient FRET pair of fluorescent proteins used by our lab, CyPet and YPet, were genetically fused to RanGAP1c and Ubc9, members of the SUMOylation pathway. During the purification process, we extracted some sample post-lysing of the *E. coli* bacterial cells we grew them in, to factor as "unpurified" proteins, given that they have yet to be subjected to column chromatography washing out of cell lysate proteins. The fully purified K_d and Em_{FRET} values were: 0.1010 ± 0.01534 μM and 2.428 ± 0.07133 x 10^5 RFU for 0.1 μM, 0.0986 ± 0.01629 μM and 4.773 ± 0.1295 x 10^5 RFU for 0.2 μM, 0.0936 ± 0.02764 μM and 12.26 ± 0.4486 x 10^5 RFU for 0.5 μM, 0.1013 ± 0.03930 μM and 23.82 ± 0.9647 x 10^5 RFU for 1.0 μM, and 0.1103 ± 0.04745 μM and 36.19 ± 1.536

x 10^5 RFU for 1.5 µM CyPet-RanGAP1c. The unpurified K_d and Em_{FRET} values were: 0.1016 ± 0.02443 µM and 1.308 ± 0.04085 for 0.05 µM, 0.09988 ± 0.02390 µM and 2.447 ± 0.07524 for 0.1 µM, 0.09616 ± 0.02348 µM and 13.57 ± 0.3915 for 0.5 µM, and 0.1001 ± 0.02919 µM and 24.63 ± 0.7893 for 1.0 µM unpurified CyPet-RanGAP1c. Both sets of K_d's and Em_{FRET}'s are of comparable value, which goes to show that purification is not necessary for use of our quantitative FRET method.

Chapter 3. Development of a Microfluidics Chip for Automated Processing of Samples as a First Step towards Integrating Quantitative FRET into a Microfluidics Imaging Device

3.1 Introduction

Proteins are key biomolecules involved in a vast number of processes within the human body. While not all of them require it, a vast number of proteins require post-translational modification, addition or removal of peptides or functional groups, in order to reach full functionality. One of the most well known post-translational modifiers is ubiquitin, which marks proteins for proteosomal degradation through an enzymatic three step cascade. Small ubiquitin-like modifier is another PTM that operates through a similar three step cascade, SUMOylation, but instead of leading proteins to their breakdown, modifies them for their biological function within cells. SUMO and its pathway components play a role in the initiation and progression of a variety of diseases.

In order to understand the mechanisms of protein pathways, the Liao lab employs quantitative Förster Resonance Energy Transfer (qFRET) technology to determine the reaction rate constants of SUMOylation. QFRET is one of the biophysical techniques used for quantitative assessment of reactions, and its competitors are Isothermal Titration Calorimetry (ITC) and Surface Plasmon Resonance (SPR). ITC is a good tool for determination of reaction parameters through measurement of thermodynamic change in a reaction mix, but it's high protocol precision threshold makes it failure prone, only one sample can realistically be run at a time, and also requires the use of large quantities of proteins. SPR is more versatile in that with the same ligand immobilized chip,

determination of binding and dissociation constants through real-time measurement of change in the resonance angle on a metal surface can be performed back to back. By utilizing microfluidic channels, the SPR chip reduces the amount of sample needed, and increase the exposure of proteins in solution to the ligands. The limitations of SPR are that it cannot differentiate between specific and non-specific binding, cannot determine a measurement from proteins of less than 20kDa without high density of immobilized ligands, and that it runs on a sample by sample basis. QFRET determines reaction rate constants through measuring FRET signal from a solution of proteins fluorescently tagged with a FRET pair. By correlating observed fluorescent signal obtained through a multi-well plate reader with bound and unbound concentrations, the reaction rate constants are determined. One of the issues with FRET measurements, as with the other biophysical methods is sample preparation, since controlled experiments require set concentrations of sample. Considering the well plate for fluorescent measurement can take up to 384 samples at once, it is advantageous to measure multiple solutions simultaneously. However, the process of diluting samples, and loading them into the individual wells is long, and depending on the skill level of the researcher, may generate mistakes.

In order to overcome human error, a microfluidics device for processing sample dilution, mixing, and ultimately fluorescence measurement was devised. Microfluidics is a welcome addition to the field of biotechnology, after having made an impact in other areas of science.[43,44,45] The device consists of two main components, the microfluidics chip with pumping apparatus, and the imaging platform. At the core of the microfluidics

lies the automated program, which given user input on the concentration of each solution for the desired measurement, would approximate how many cycles of pumping are required to appropriate an accurate dilution. Once mixing of both dilutions was done, the chip would then be imaged for fluorescence. The data for fluorescence intensity would be presented to the user, who then selects the regions of fluorescence within the image to process, and the program would run the measured values through equations developed by previous lab students to determine true FRET signal, and the dissociation constant, K_d.[25] In automating the process, we decrease processing time for setup of assays, as well as maintain as close to in vivo measurements as in vitro can reach. Herein we report design and testing of the first generation of microfluidics chip with the intention of measuring FRET signal for quantitative assessment.

3.2 Materials and methods

Initial Planning

Initial planning included several prototypes that were key to development for the final form of the device. Since the main purpose of the device was to measure fluorescence from a series of diluted solutions that were mixed previously within the device, the first priority was that the inputs mixed properly. This resulted in a loop design as the core form of the microfluidics portion, with spacing that supported half dilutions for the sake of simplicity in design. One of the earlier ideas included a central collection chamber for the purpose of gathering solution in one spot for easier imaging access, but the idea was scrapped due to concern about efficient removal of solution after imaging. After consideration of the need for two separate samples to be processed in parallel in order to

prove comparable to our lab's current assay procedure, a solution to the design was found. We finalized design of the fluidic portion to center around two intersecting loops, so that we could individually dilute the solutions, then mix them together in a wider loop of the perimeter, or the smaller loop of the intersecting portion, which accounted for variation of camera focus. The inefficient use of space in the center led to some rethinking. After careful consideration of placement, the final design of the first generation chip is as shown in **Figure** 8.

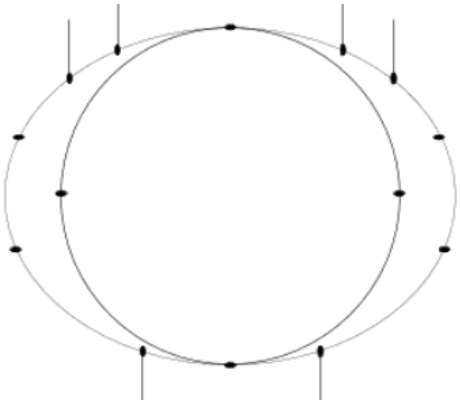

Figure 9. Preliminary design of intersecting loops. Designed to have capacity to dilute two separate solutions, then mix them together.

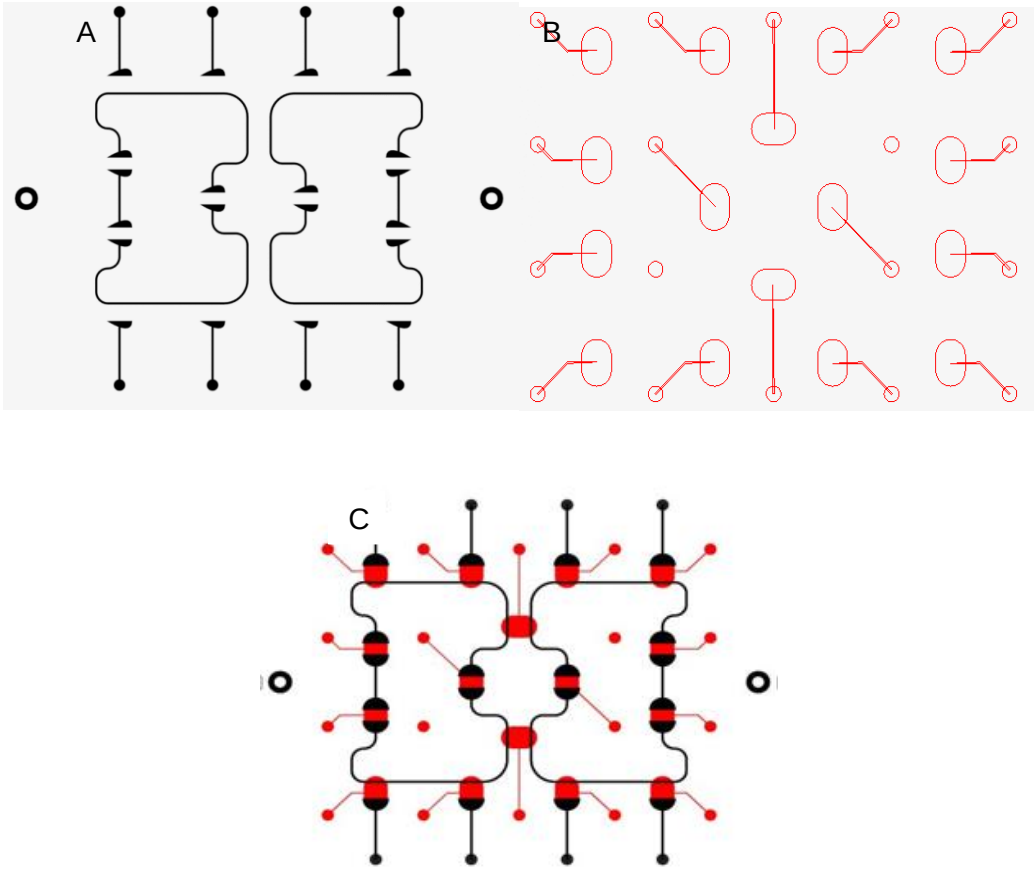

Figure 10. Final design. A). Fluidic layer, designed for processing of 2 separate samples. B). Pneumatic layer, designed for actuation of valves to mix samples using 14 lines of control. C). Overlay of fluidic on pneumatic layer.

The chip was designed with three layers in mind: the top fluidic layer where all of the fluidic transport and imaging would take place, the middle PDMS layer which will facilitate transport of fluid, and the pneumatic layer on the bottom, which directs fluidic flow in the top layer with pressure applied to the PDMS.

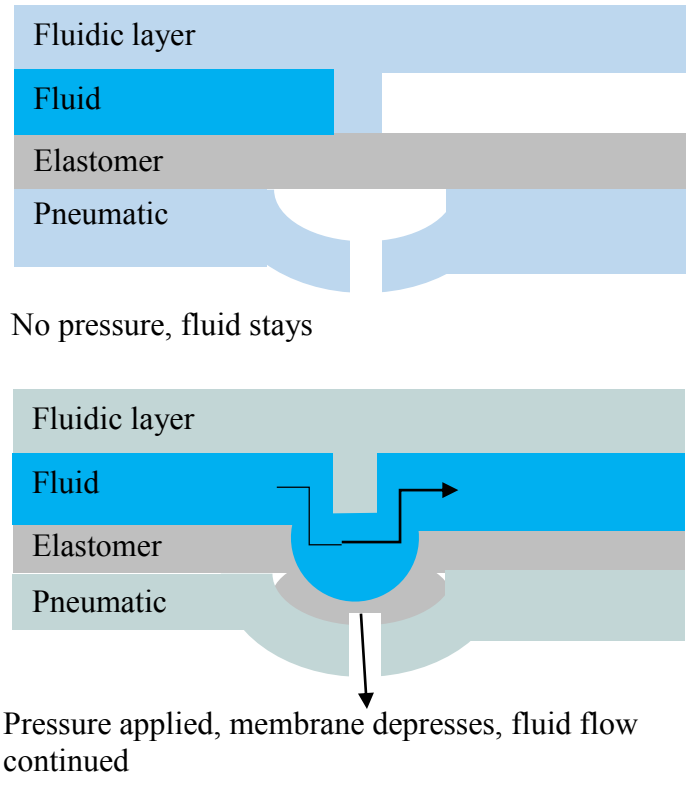

Figure 11. Diagram of monolithic membrane valve operation. Fluid moves around in the top layer, but is stopped by discontinuities. Upon application of pressure from the pneumatic layer, the PDMS is drawn down, and fluid can continue to flow.

A computer program would control a pressure pump, which directs the flow of fluidic motion with actuation of valves to temporarily disrupt a PDMS barrier in the fluidic layer. The program was intended to have the capability to mix two separate solutions individually, with no leakage from one loop to the next, and the ability to vary the number of repetition of loops to account for differing viscosities of solutions. Computer commands enter the 34-pin controller, which sends a 5V signal to the Darlington arrays, flipping the switches inside between off or on. If the switch is turned on, the amplified signal leaves the Darlington array, and is subsequently applied to the solenoid valves. Without signal, the valves stay closed, but once the threshold current is

achieved, the valves activate, applying pressure to the chip. The 34-pin controller has more lines of control than we are using with this model, and leave room for expansion of the number valves utilized, or spare lines of control should some start to falter in performance.

Table 1. Pin Assignments

Signal	Pin	Connector	Pin	Signal
P1.0	1		2	GND
P1.1	3		4	P2.0
P1.2	5		6	GND
P1.3	7		8	P2.1
P1.4	9		10	GND
P1.5	11		12	P2.2
P1.6	13		14	GND
P1.7	15		16	P2.3
P0.0	17		18	GND
P0.1	19		20	P2.4
P0.2	21		22	GND
P0.3	23		24	P2.5
P0.4	25		26	GND
P0.5	27		28	P2.6
P0.6	29		30	GND
P0.7	31		32	P2.7
+5V	33		34	+5V

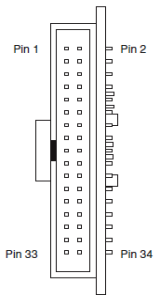

Figure 12. Schematic of pin distribution. Out of 32 possible output pins, only 14 were used to control the microfluidic chip. Possible to expand to a 4 sample chip, run two separate 2 samples chips, or introduce higher complexity of commands in later design iterations while keeping same controller.

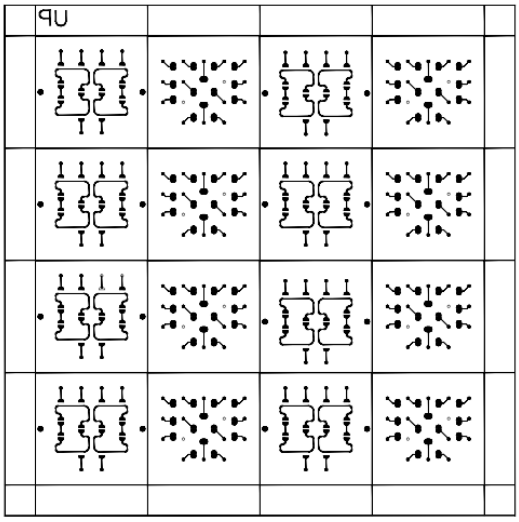

Figure 13. Inverted photomask with chip design. Size of chip allowed for multiple copies on same pre-coated glass wafer containing glass, protective coating, and photosensitive coating.

Fabrication

Once the blueprint was finalized, a custom mask was ordered in order to help us imprint the design on a glass wafer pre-coated with photoresist and chrome (**Figure 11**). The design was reversed colorwise so that the chip details were clear on a black background. Once the photomask arrived, we used it to imprint the chip design onto the pre-coated wafer using photolithography. In as dark a room as possible, we treated the glass wafer with photomask on top using photolithography. After exposure, the wafer was washed, and our desired design was imprinted into the photoresist, now with protective chrome layer exposed in the pattern of the blueprint.

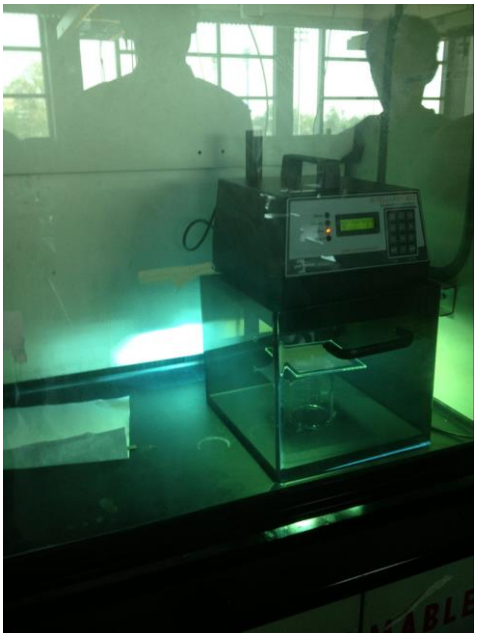

Figure 14. Photolithography. Standard method of imprinting design into glass substrate using UV light to develop a photosensitive layer for later etching.

For the next step in the fabrication process, we brought the glass wafer to the clean room in the Nanofabrication Facility on campus. The wafer was treated with chromium etchant to remove the protective chrome layer from the glass in the pattern of our photomask. After washing off the etchant solution with acetone and water, the wafer was ready for etching by hydrofluoric acid. Hydrofluoric acid dissolves glass at a rate of 7µL per minute, so attaining the desired channel depth of 70µm, we let the wafer sit in the hydrofluoric bath for 10 minutes. After cleaning off the hydrofluoric acid with water, the wafer was developed with photolithography sans mask to remove the photo resistant layer, chrome etch to remove the protective chrome, and acetone to wash it all off. Having removed all else, our glass wafer with chip design etched onto it remained.

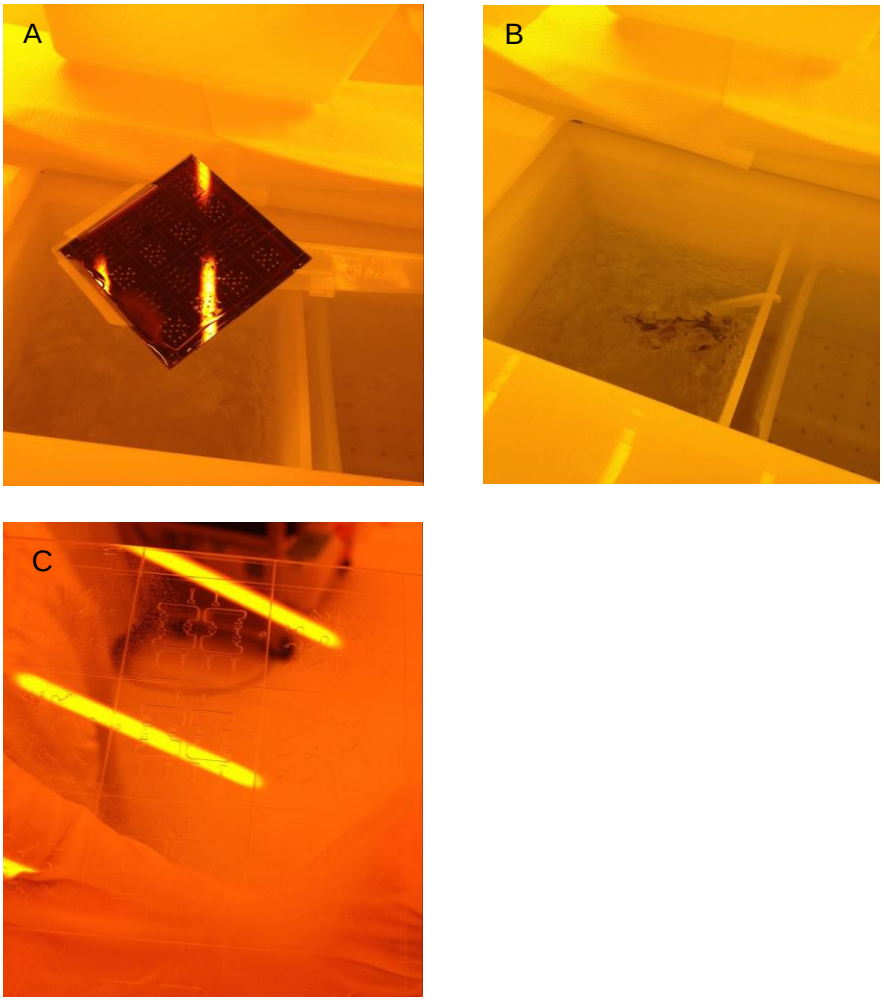

Figure 15. Etching process. A). Wafer with photoresist after applying chrome etch to remove protective chrome layer. B). Etching of wafer in hydrofluoric acid at 10µM/min. C). Etched wafer after removing photoresist and chrome layers.

To prepare the glass layers for assembly, we had to drill the appropriate holes for both layers. This was accomplished with the help of the Grover lab's CNC drill, and Python code for directing it. Four input and four output holes were drilled into the fluidic layer, while the pneumatic layer had 16 holes drilled in for the various lines of valve control. Due to the size of our design, multiple chips were able to be etched onto a single wafer, so we cut out one set of chip layers with a diamond tipped rod. The fragment was

joined to a disposable glass piece using resin, and Milli-Q water was pipetted onto the fragment until a layer of water covered it. This covering was necessary to dissipate heat from the drill, and to contain the pieces of glass removed during the drilling process for simpler cleanup. Once drilling finished, the resin was removed by washing under water. After separating the fluidic and pneumatic layers with the diamond tipped tool, we then sandwiched a small piece of PDMS between the two glass layers, and let it sit for a few hours to ensure that the seal would hold. The excess PDMS was cut off to complete the chip.

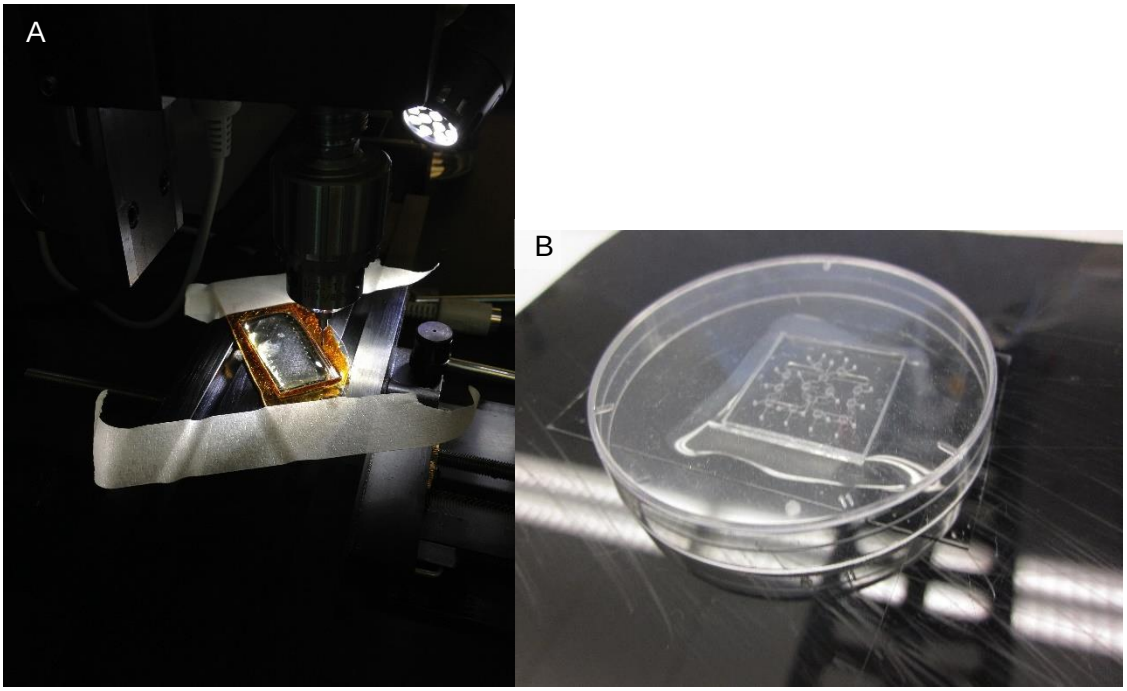

Figure 16. Final stages of fabrication. A). Drilling with the CNC mill. B). Fusing of the three layers: fluidic, PDMS, and pneumatic.

The chip moves fluid through itself using a series of actuating valves driven by pressure from plastic tubing connected to an array of solenoid valves. Due to scaling of

the device, the tubes could not reliably stay directly in contact with the pneumatic layer. Thus, we designed a "holder" in Solidworks to serve as interface between the tubing and chip. A cube served as the base structure for the holder, with indentations of slightly larger circumference than the tubing echoed in the same pattern as the valves of the pneumatic layer. After finalizing the design, the holder was printed via a 3D printer, and sanded down to accommodate for printing error, which took form in a rounded surface. The tubing was measured out to a length of 7 inches to accommodate for movement of the chip-holder apparatus. Hot glue was used to seal the tubing inside of the indentations, assuring zero leakage of pressure.

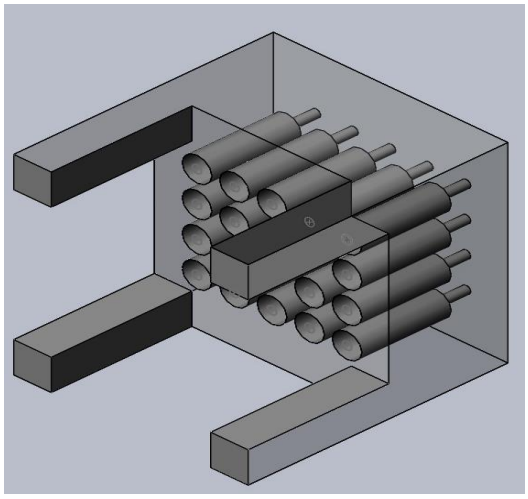

Figure 17. Initial design of chip holder. Chip designed to sit on top of holder, which accounted for low flexibility of the tubing to fix tubes in place to ensure efficient transmission of pressure.

The core component of operating the chip is pressure, and to fulfill the need for actuation of pressure as a means of transport through the chip, we needed to be able to control where the pressure was applied in a timely manner. Therefore we employed the use of circuitry to facilitate running our chip. From the computer, commands are sent to

the USB-6501 OEM controller from National Instruments, with 24 bit control. For ease of assembly, a special clip for linkage with the controller was attached to rainbow wire, chosen for the variation of color, deemed helpful in differing lines of control. The wires were lined up with two Darlington arrays in parallel, used as signal amplification for control of valves being on or off. Across from the rainbow wire ran the wires of the solenoid valve assembly. Altogether, the controller sends signal through the Darlington arrays to the solenoid valves, for whether they should or should not apply pressure. Lastly, the solenoid valve array was connected to a pressure pump as a vacuum source, and the individual valves were bound by tubing to their respective pneumatic layer valves within the holder.

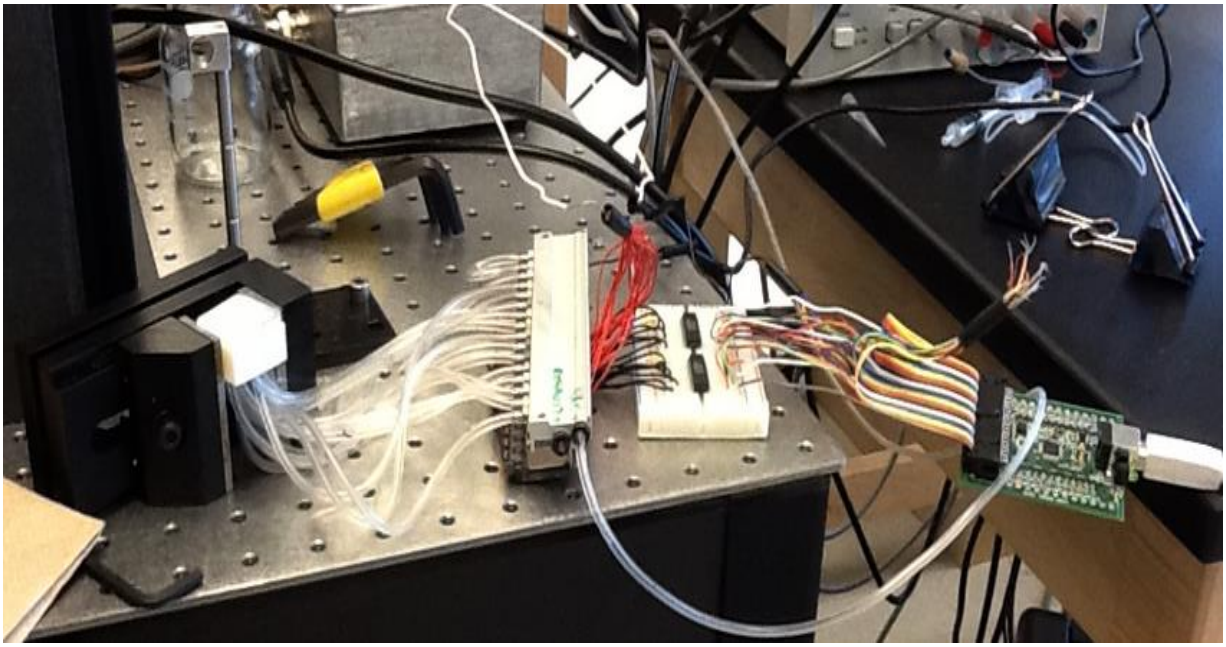

Figure 18. Fully linked microfluidic set. From left to right: chip, holder, pressure tubing, solenoid valve array, Darlington arrays, rainbow wire, and controller.

Software for operation of the chip consisted of four Labview (National Instruments) programs we adopted from the Grover lab: listener, manual, ocw, and controller. Manual, as the name implies, was a visual representation of the solenoid valve apparatus. By clicking on individual valves, you could turn them on or off, with a lit up valve meaning on, and darkened representing off. If a programmed set of controls was running, you observed the valves turning on and off in the sequence given. Upon spotting discrepancy, adjustments could be made to the hardware. Listener is a program communicating from the computer code to the lines of control on the controller. To be specific, the controller itself had more lines of control than we were using, and listener allowed us to choose which lines of control were to be active, and which were to be ignored in the processing of commands from the computer. Ocw reads the command script. Controller embodied the code used to execute commands to the chip system. It consisted of a front page for user input of commands, and a back page of the actual pathing of commands and code. The front page contains a drop down menu for which programmed loops to run on each side of the chip, as well as a manual input for the number of iterations to run.

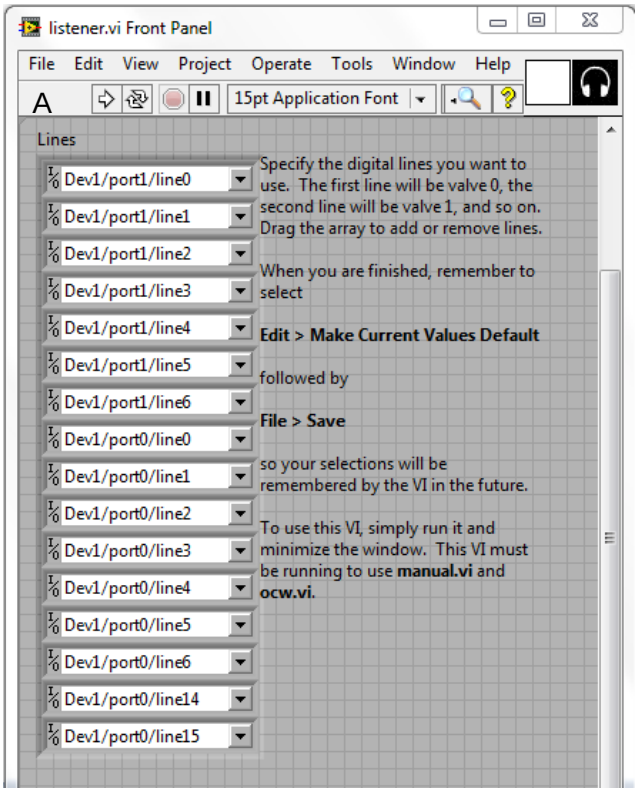
listener.vi Front Panel
File Edit View Project Operate Tools Window Help
15pt Application Font
A
Lines
Dev1/port1/line0
Dev1/port1/line1
Dev1/port1/line2
Dev1/port1/line3
Dev1/port1/line4
Dev1/port1/line5
Dev1/port1/line6
Dev1/port0/line0
Dev1/port0/line1
Dev1/port0/line2
Dev1/port0/line3
Dev1/port0/line4
Dev1/port0/line5
Dev1/port0/line6
Dev1/port0/line14
Dev1/port0/line15
Specify the digital lines you want to use. The first line will be valve 0, the second line will be valve 1, and so on. Drag the array to add or remove lines.
When you are finished, remember to select
Edit > Make Current Values Default
followed by
File > Save
so your selections will be remembered by the VI in the future.
To use this VI, simply run it and minimize the window. This VI must be running to use manual.vi and ocw.vi.

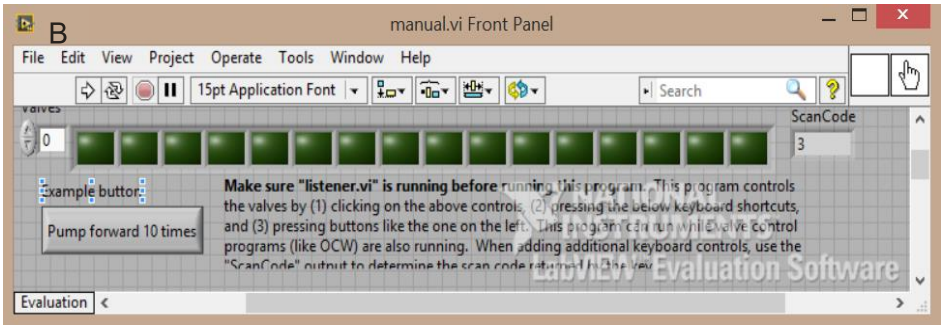
B
manual.vi Front Panel
File Edit View Project Operate Tools Window Help
15pt Application Font
Search
ScanCode
3
Example button
Pump forward 10 times
Make sure "listener.vi" is running before running this program. This program controls the valves by (1) clicking on the above controls, (2) pressing the below keyboard shortcuts, and (3) pressing buttons like the one on the left. This program can run while valve control programs (like OCW) are also running. When adding additional keyboard controls, use the "ScanCode" output to determine the scan code returned by the key.
LabVIEW Evaluation Software
Evaluation

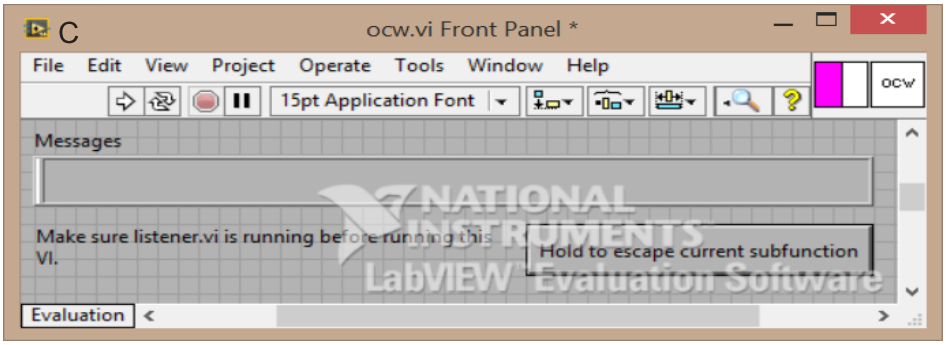
C
ocw.vi Front Panel *
File Edit View Project Operate Tools Window Help
15pt Application Font
ocw
Messages
Make sure listener.vi is running before running this VI.
Hold to escape current subfunction
NATIONAL INSTRUMENTS
LabVIEW Evaluation Software
Evaluation

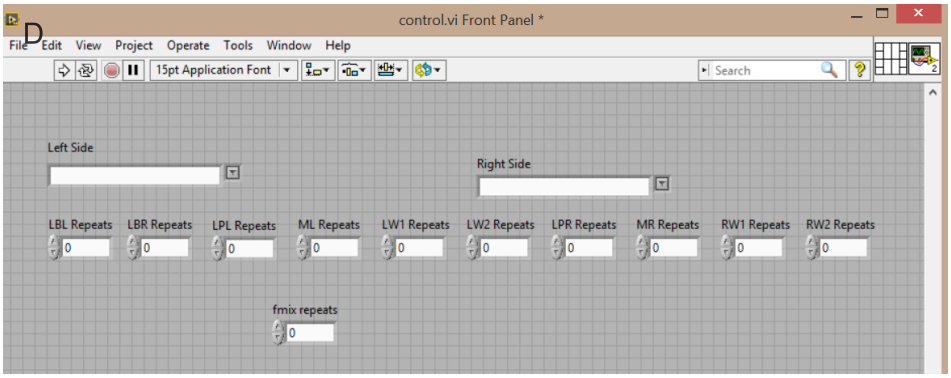

Figure 19. Programs for Chip Control. A). Listener aligns computer lines of control to pins in the controller. B). Manual gives visual representation of which lines of control are active, and can manually activate them. C). Ocw runes the scripts. D). Control has drop down menus for each chip loop, with relevant commands, and user input of how many iterations to run.

Testing of device

Once all the parts were assembled, initial testing could begin. We started with simple water testing to see if the chip would actually allow fluid flow. Since the PDMS was stuck to the glass layers, we loosened up the valves using a syringe. After a period of about an hour of continually applying a small volume of water to the input channels, and pressure using the syringe, we finally saw some water exiting the output channels. Over the course of another few hours, we were able to see water pumping through the entire device on the condition that all valves were exposed to water consistently. Several iterations of loading the chip with water and emptying it were performed, and the working volume of each loop was determined to be ~0.5µL. The next stage of testing involved observing the rate at which the chip could mix two separate solutions using food color-dyed water. One drop each of blue and yellow food coloring were added to separate 1.5 mL eppendorf tubes, filled to max capacity with DI water. Within 20

minutes of mixing, the individual dilutions were visually uniform, and after another 20 minutes for whole chip mixing, the entire outer loop was a nice green color.

Factoring in the fact that with all of the tubing underneath the microfluidics chip would interfere with imaging of the device, and the need to improve the efficiency of the chip, we redesigned it a bit. The first optimization was reallocating the fluidic and pneumatic holes to the outside, to leave room for fluorescence reading on the fluidic side. By reducing the thickness of the PDMS layer for the second optimization, we hoped that the pressure from the pneumatic side would more easily disrupt the PDMS membrane, allowing for faster operation for better results. Additionally, a new holder was made to accommodate the new chip design. Unfortunately, the second generation chip has not been able to work when applied to the current setup, and additional tweaking would be required to start testing operations.

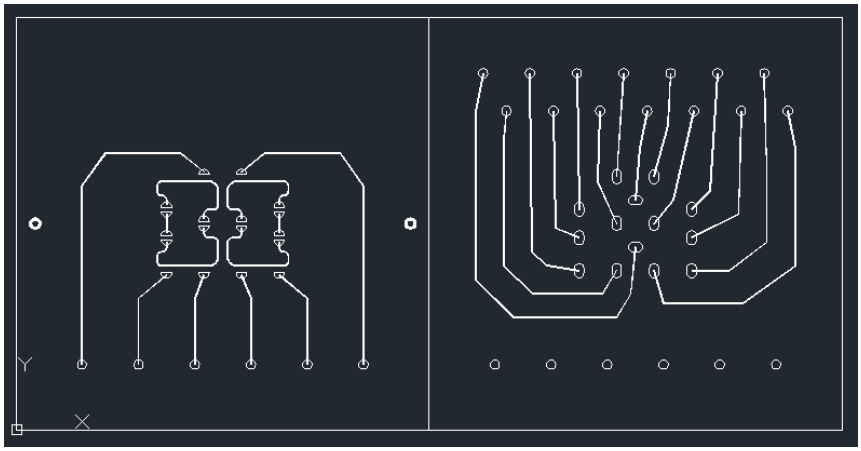

Figure 20. Redesigned chip blueprint. Remodeled design attempts to integrate both pneumatic and fluidic layes onto the same side, allow of imaging of samples along the channels with little to no obstruction by tubing.

3.3 Results

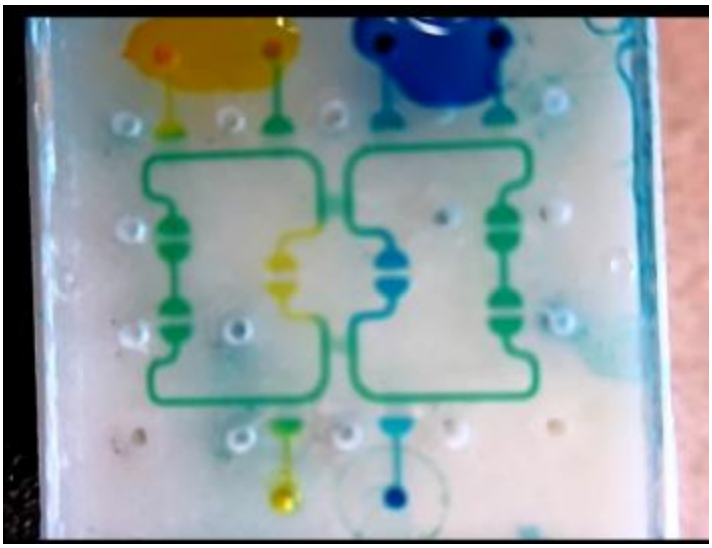

Figure 21. Colored dye test for chip. Left loops loaded with yellow dye, right loops loaded with blue dye. Mixing both loops produced green dye.

From the results of the test, several issues were identified. First, the chip took more than an hour of continuously pumping air and water through to get ready for any sort of testing. One possible explanation was the thickness of our PDMS was more than the solenoid valves could displace from a dry state. Another is that the pressure was not properly transmitted to the pneumatic layer, which was validated by the food coloring experiments. When mixing the blue and yellow loops, it was easy to observe that the blue side was mixing into the yellow much faster than the yellow was mixing into the blue. As such, the spread of green started with the interface of blue entering yellow, and continued until the outer loop was about two-thirds light green and one-third blue. Uniform coloring occurred a few minutes later.

3.4 Discussion

The original goal of this project was to create a device for user-controlled dilution and mixing of samples, followed by measurement of FRET interaction for quantification using our lab's quantitative FRET technique. We report that a microfluidics chip was constructed with monolithic membrane valves and pumps, as intended. It was tested three times, once for determination of preparation parameters, a second time for quantitative evaluation of operation, and lastly for quantitative assessment of its abilities. The first test illustrated foremost that the components used made preparation long, and restricted the ability to further test. By adding food coloring to water samples for the second test, we were able to get a visual idea of where exactly the chip was deficient. We observed that one side more easily was mixing with the other color, which can be compensated by running the chip for a longer period of time. However, the fact that other solutions, especially those found in a wet laboratory setting, are likely to be more viscous that water, is a point to consider. Finally, the last test gave us a numerical value for the efficiency of our chip's dilutions. At 112 μM, instead of 182, the resultant dilution is thirty percent, which is significantly lower than the intended 50%. Reasoning for all these issues has been allocated to the thick PDMS layer in the middle. Although the efficiency of the newly fabricated chip has yet to be tested, we are confident it will perform much better than its predecessor.

Chapter 4. Future goals

4.1 Regarding Protein Assay Studies

Now that we have established purification is not necessary for quantitative FRET measurement of the E2 and substrate interaction of the SUMOylation pathway, it would be wise to test it with all pathway components to confirm the results are not circumstantial. Additionally, we can extend this to ubiquitination and other pathways as well. If for any reason the purification process of future proteins goes awry, we can then employ the method of not purifying to enable continuation of experiments without having to search for alternate purification methods. Depending on the protein expressed, the process of column chromatography can take between one and eight hours, so the knowledge that it can be avoided is much appreciated. Granted, some purifications take a large number of hours to complete because the protein was improperly expressed, but there's no harm in checking a protein sample for activity over plain trashing it because you believe it to be wholly unusable.

4.2 Regarding the Microfluidics Device

Once testing of the second generation chip is complete, determination of further steps to complete the device will be found. During the initial planning stages, replication of the adjustable laser and photomultiplier tube camera within our lab's Flexstation II 384 (**Figure 21**) was discussed as an option for developing an imaging platform for the device. Unfortunately, the manual did not indicate which ones they were using, and the company representative did not give any hints. We instead approached other companies, asking for the price of their lasers and cameras, which turned out to be price quotes

between $5000 and $7000 for each one. For those that wish to continue this project, it is advised to attempt to buy needed parts for secondhand sources, which will no doubt be cheaper than fresh industry-grade equipment. Completion without the imaging platform is also an option, as once we get our chip to run as quickly, it will serve as hands free dilution of samples, which allows lab students more time to do other tasks, and can even be run by inexperienced members too.

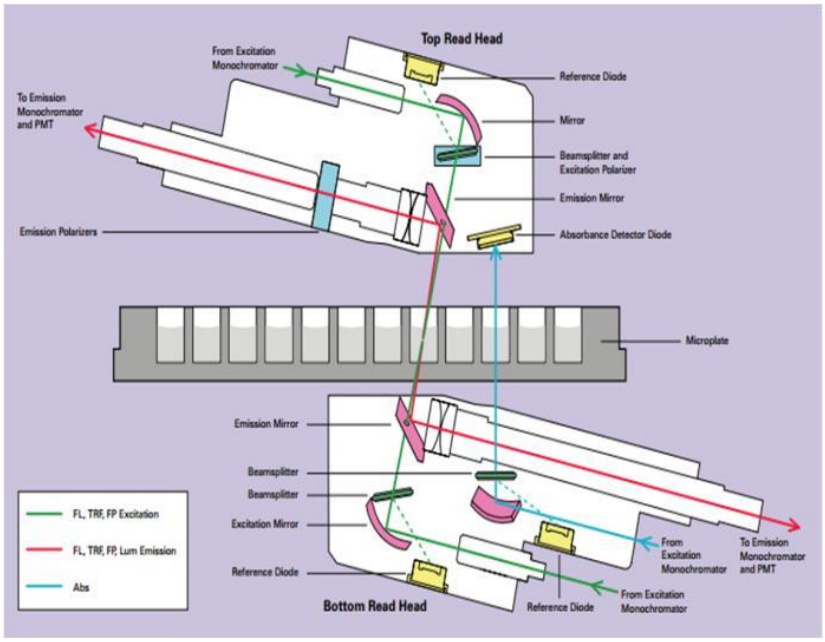

Figure 22. The inside of a Flexstation II 384. Important parts to replicate are: clear bottom well plate, excitation source, light detection module, and mirror orientation.

References

1. Mann, M. and O.N. Jensen. "Proteomic analysis of post-translational modifications." *Nat Biotech* (2003) **2,** p. 255-261.

2. Welchman, R. L., Gordon, C. & Mayer, R. J. "Ubiquitin and ubiquitin-like proteins as multifunctional signals." *Nature reviews. Molecular cell biology* (2005) **6**, p. 599-609.

3. Schlesinger, D.H., G. Goldstein, and H.D. Niall, "Complete amino acid sequence of ubiquitin, an adenylate cyclase stimulating polypeptide probably universal in living cells." *Biochemistry* (1975) **14,** p. 2214-2218.

4. Pickart, C.M. "Mechanism Underlying Ubiquitination" *Annual Review of Biochemistry* (2001) **70**, p. 503-533.

5. Mukhopadhyay, D., and Riezman, H. "Proteasome-Independent Functions of Ubiquitin in Endocytosis and Signaling" *Science* (2007) **315**, p. 201-205.

6. Hoege, C., Pfander, B., Moldovan, G.L., Pyrowolakis, G., and Jentsch, S. "RAD6-dependent DNA repair is linked to modification of PCNA by ubiquitin and SUMO" *Nature* (2002) **419**, p. 135-141.

7. Kerscher, O., Felberbaum, R., and Hochstrasser, M. "Modification of Proteins by Ubiquitin and Ubiquitin-Like Proteins" *Annual Review of Cell and Developmental Biology* (2006) **22**, p. 159-180.

8. Meluh, P.B., and Koshland, D. "Evidence that the MIF2 gene of Saccharomyces cerevisiae encodes a centromere protein with homology to the mammalian centromere protein CENP-C" *Molecular Biology of the Cell* (1995) **6**, p. 793-807.

9. Matunis, M.J., Coutavas, E., and Blobel, G. "A Novel Ubiquitin-like Modification Modulates the Partitioning of the Ran-GTPase-activating Protein RanGAP1 between the Cytosol and the Nuclear Pore Complex" *The Journal of Cell Biology* (1996) **135**, p. 1457-1470.

10. Shen, Z., Pardington-Purtymun, P.E., Comeaux, J.C., Moyzis, R.K., and Chen, D.J. "UBL1, a Human Ubiquitin-like Protein Associating with Human RAD51/RAD52 Proteins" *Genomics* (1996) **36**, p. 271-279.

11. Johnson, E.S. "Protein Modification by SUMO" *Annual Review of Biochemistry* (2004) **73,** p. 355-382.

12. Melchior, F. "SUMO- Nonclassical Ubiquitin" *Annual Review of Cell and Developmental Biology* (2000) **16**, p. 591-626.

13. Jackson, P.K. "A new RING for SUMO: wrestling transcriptional responses into nuclear bodies with PIAS family E3 SUMO ligases" *Genes and Development* (2001) **15**, p. 3053-3058.

14. Pichler, A., Gast, A., Seeler, J.S., Dejean, A., and Melchior, F. "The Nucleoporin RanBP2 Has SUMO1 E3 Ligase Activity" *Cell* (2002) **108,** p. 109-120.

15. Kagey, M.H., Melhuish, T.A., and Wotton, D. "The polycomb protein Pc2 is a SUMO E3" *Cell* (2003) **113,** p. 127-137.

16. Guo, D., Li, M., Zhang, Y., Yang, P., Eckenrode, S., Hopkins, D., Zheng, W., Purohit, S., Podolsky, R.H., Muir, A., Wang, J., Dong, Z., Brusko, T., Atkinson, M., Pozzilli, P., Zeidler, A., Raffel, L.J., Jacob, C.O., Park, Y., Serrano-Rios, M., Larrad, M.T.M., Zhang, Z., Garchon, H., Bach, J., Rotter, J.I., She, J., and Wang, C. "A functional variant of SUMO4, a new IKBα modifier, is associated with type 1 diabetes" *Nature Genetics* (2004) **36**, p. 837-841.

17. Li, Y., Wang, H., Wang, S., Quon, D., Liu, Y., and Cordell, B. "Positive and negative regulation of APP amyloidogenesis by sumoylation" *PNAS* (2003) **100**, p. 259-264.

18. Bettermann, K., Benesch, M., Weis, S., and Haybaeck, J. "SUMOylation in carcinogenesis" *Cancer Letters* (2012) **316,** p. 113-125.

19. Schimdt, D., Müller, S. "Members of the PIAS family act as SUMO ligases for c-Jun and p53 and repress p53 activity" *PNAS* (2002) **99**, p. 2872-2877.

20. Pierce, M.M., Raman, C.S., and Nall, B.T. "Isothermal Titration Calorimetry of Protein-Protein Interactions" *Methods* (1999) **19**, pp. 213-221.

21. Schuck, P. "Use of Surface Plasmon Resonance to Probe the Equilibrium and Dynamic Aspects of Interactions between Biological Macromolecules" *Annual Review of Biophysics: Biomolecular Structures* (1997) **26**, pp. 541-566.

22. Ahmed, F.E., Wiley, J.E., Weidner, D.A., Bennerup, C., and Mota, H. "Surface Plasmon Resonance (SPR) Spectrometry as a Tool to Analyze Nucleic Acid-Protein Interactions in Crude Cellular Extracts" *Csncer Genomics and Proteomics* (2010) **7**, pp. 303-309.

23. Huh, W., Falvo, J.V., Gerke, L.C., Carroll, A.S., Howson, R.W., Weissman, J.S., and O'Shea, E.K. "Global analysis of protein localization in budding yeast" *Nature* (2003) **425**, p. 686-691.

24. Johnsson, K. "Visualizing biochemical activities in living cells" *Nature Chemical Biology* (2009) **50**, p.63-65.

25. Ciruela, F. "Fluorescence-based methods in the study of protein-protein interactions in living cells" *Current Opinion in Biotechnology* (2008) **19**, p. 336-343.

26. Förster, T. "Energiewanderung und Fluoreszenz" *Naturwissenschaften* (1946) **33**, p.166-175.

27. Förster, T. "Energy migration and fluorescence" *Journal of Biomedical Optics* 17 (2011), 011002.

28. Stryer, L. "Fluorescence Energy Transfer as a Spectroscopic Ruler" *Annual Review Biochemistry* (1978) **47**, pp. 819-846.

29. Berney, C., and Danuser, G. "FRET or No FRET: A Quantitative Comparison" *Biophysical Journal* (2003) **84**, pp 3992-4010.

30. Song, Y., Rodgers, V.G.J., Schultz, J.S., and Liao, J. "Protein Interaction Affinity Determination by Quantitative FRET Technology" *Biotechnology and Bioengineering* (2012) **109,** p. 2875-2883.

31. Lois, L.M., and Lima, C.D. "Structures of the SUMO E1 provide mechanistic insights into SUMO activation and E2 recruitment to E1" *The EMBO Journal* (2005) **24,** p. 439-451.

32. Miyawaki, A., Llopis, J., Heim, R., McCaffery, J.M., Adams, J.A., Ikura, M., and Tsien, R.Y. "Fluorescent indicators for Ca^{2+} based on green fluorescent proteins and calmodulin" *Nature* (1997) **388**, p. 882-887.

33. Wang, L., Yan, R., Huo, Z., Wang, L., Zeng, J., Bao, J., Wang, X., Peng, Q., and Li, Y. "Fluorescence Resonant Energy Transfer Biosensor Based on Upconversion-Luminescent Nanoparticles" *Angewandte Chemie* (2005) **44**, p.6054-6057.

34. Giepmans, B.N.G., Adams, S.R., Ellisman, M.H., Tsien, R.Y. “Review – The fluorescent toolbox for assessing protein location and function” *Science* (2006) **312**, p.217-224.

35. Song, Y., Madahar, V. & Liao, J. “Development of FRET Assay into Quantitative and High-throughput Screening Technology Platforms for Protein-Protein Interactions” *Ann Biomed Eng* (2011) **39**, p. 1224-1234.

36. Liu, Y., Song, Y., Madahar, V. & Liao, J. “Quantitative Forster resonance energy transfer analysis for kinetic determinations of SUMO-specific protease” *Anal Biochem* (2012) **422**, pp14-21.

37. Liu, Y. & Liao, J. “Quantitative FRET (Forster Resonance Energy Transfer) analysis for SENP1 protease kinetics determination” *J Vis Exp*, e4430 (2013)

38. Jiang, L. *et al.* Internal calibration forster resonance energy transfer assay: a realtime approach for determining protease kinetics.” *Sensors (Basel)* (2013) **13**, p. 4553-4570.

39. Song, Y. & Liao, J. “An In Vitro Forster Resonance Energy Transfer-Based High Throughput Screening Assay for Inhibitors of Protein-Protein Interactions in SUMOylation Pathway.” *Assay Drug Dev Technol* (2011).

40. Liu, Y., Song, Y., Jiang, L. & Liao, J. “Quantitative analysis of FRET assay in biology.” *Frontiers in Biology* (2012) **7**, p. 57-64.

41. Manz, A., Harrison, D.J., Verpoorte, E.M.J., Fettinger, J.C., Paulus, A., Lüdi, H., and Widmer, H.M. “Planar chips technology for miniaturization and integration of separation techniques into monitoring systems: Capillary electrophoresis on a chip” *Journal of Chromatography A* (1992) **593,** p. 253-258

42. Whitesides, G.M. “The origins and the future of microfluidics” *Nature* (2006) **442**, p. 368-373.

43. Duffy, D.C., McDonald, J.C., Schueller, J.A., and Whitesides, G.M. “Rapid Prototyping of Microfluidic Systerms in Poly(dimethylsiloxane)” *Anal. Chem.*, (1998) **70**, p. 4974-4984.

44. Xia, Y., and Whitesides, G.M. “Soft Lithography” *Angewandte Chemie* (1998) **37**, p. 550-575.

45. Unger, M.A., Chou, H.P., Thorsen, T., Scherer, A., and Quake, S.R. "Monolithic Microfabricated Valves and Pumps by Soft Lithography" *Science* (2000) **288**, p.113-116.

46. Thorson, T., Maerkl, S.J., and Quake, S.R. "Microfluidic Large-Scale Integration" *Science* (2002) **18**, p. 580-584.

47. Grover, W.H., Skelley, A.M., Liu, C.N., Lagally, E.T., Mathies, R.A. "Monolithic membrane valves and diaphragm pumps for practical large-scale integration into glass microfluidic devices" *Sensors and Actuators B* (2003) **89**, p. 315-323.

48. Cho, S.K., Moon, H., and Kim, C. "Creating, Transporting, Cutting, and Merging Liquid Droplets by Electrowetting-Based Actuation for Digital Microfluidic Circuits." *Journal of Microelectromechanical Systems* (2003) **12**, p. 70-80.

49. Park, J., Hardy, M., Kang, S.J., Barton, K., Adair, K., Mukhopadhyay, D.K., Lee, C.Y., Strano, M.S., Alleyne, A.G., Georgladis, J.G., Ferreira, P.M., and Rogers, J.A. "High-resolution electrohydrodynamic jet printing" *Nature Materials* (2007) **6**, p. 782-789.

50. Khademhosseini, A., Langer, R., Borenstein, J., and Vacanti, J.P. "Microscale technologies for tissue engineering and biology" *PNAS* (2006) **103**, p. 2480-2487.

51. Nagrath, S., Sequist, L.V., Maheswaran, S., Bell, D.W., Irimia, D., Ulkus, L., Smith, M.R., Kwak, E.L., Digumarthy, S., Muzikansky, A., Ryan, P., Balis, U.J., Tompkins, R.G., Haber, D.A., and Toner, M. "Isolation of rare circulating tumour cells in cancer patients by microchip technology" *Nature* (2007) **450**, p. 1235-1239.

52. Dittrich, P.S., and Manz, A. "Lab-on-a-chip: microfluidics in drug discovery" *Nature Reviews Drug Discovery* (2006) **5**, p. 210-218.